ABSTRACT

Title of Document: COMPUTATIONAL STUDIES ON ORGANELLE-SPECIFIC YEAST MEMBRANE MODELS

Viviana Monje-Galvan, Master of Science, 2014

Directed By: Prof. Jeffery B. Klauda
Department of Chemical and Biomolecular Engineering

Computational models were built for the endoplasmic reticulum (ER), trans-Golgi network (TGN), and plasma membranes (PM) of yeast *Saccharomyces cerevisiae*. Based on experimental data, ergosterol, phosphatidic acid, phosphatidylcholine, phosphatidylethanolamine, phosphatidylserine, and phosphatidylinositol lipids were included. Lipid packing, order parameters (S_{CD}), electron density profiles (EDPs), and lipid rotation were studied for each model. The average surface area per lipid decreased from 63.82±0.03 $Å^2$ in the ER to 47.09±0.12 $Å^2$ at the PM; while the compressibility modulus (K_A) varied in opposite direction (PM>TGN>ER). The S_{CD} values were higher (more ordered) for the PM lipids than the ER and TGN membranes by a factor of 1.5. The bilayer thickness estimated from EDPs was larger for the PM (43.9±0.1 Å) than the ER or TGN (37.6±0.1 Å). These properties followed expected experimental trends and were compared against a previous model built by Jo *et al.* (*Biophys J.* **2009,** 97:50-58).

COMPUTATIONAL STUDIES ON

ORGANELLE-SPECIFIC YEAST MEMBRANE MODELS

By

Viviana Monje-Galvan

Thesis submitted to the Faculty of the Graduate School of the
University of Maryland, College Park, in partial fulfillment
of the requirements for the degree of
Master of Science
2014

Advisory Committee:
Professor Jeffery Klauda, Chair
Professor Mikhail Anisimov
Professor Amy Karlsson
Proffesor Panagiotis Dimitrakopoulos

Dedication

This thesis is dedicated to my mother and grandfather for their love and inspiration. I thank God for His countless blessings, especially for my supportive husband.

Acknowledgements

I would like to acknowledge Dr. Jeffery Klauda for his direction and patience throughout this project, and for helping me attend four conferences in which I presented my work. I would also like to thank the Center for Minorities in Science and Engineering of the University of Maryland for assisting me financially through the LSAMP Bridge to the Doctorate Fellowship.

Table of Contents

Dedication ii
Acknowledgements iii
Table of Contents iv
List of Figures v
List of Tables vi
List of Abbreviations vii
CHAPTER 1 - BACKGROUND 1
1.1 Biological membranes 1
1.1.1 Membrane Lipids 1
1.1.2 Membrane proteins 6
1.1.3 Sterols 7
1.2 Yeast membranes 8
1.2.1 Endoplasmic Reticulum (ER) 8
1.2.2 Trans-Golgi Network (TGN) 9
1.2.3 Plasma Membrane (PM) 10
1.3 Molecular Dynamics (MD) Simulations 11
1.3.1 Force Fields 12
1.3.2 Temperature and Pressure control in MD 14
CHAPTER2 - METHODS 16
2.1 Building and Equilibration techniques 16
2.2 Systems of study 17
2.2.1 Average Yeast Model (AVG-Yeast) 17
2.2.2 Complex Models 19
2.3 MD simulations settings 21
CHAPTER 3 - RESULTS AND DISCUSSION 23
3.1 SA per lipid and Compressibility modulus (K_A) 23
3.2 Electron density profiles (EDP) 25
3.3 Deuterium order parameters (S_{CD}) 29
3.4 Lipid wobble rotation – NMR relaxation times (T_1) 32
CHAPTER 4 – BROADER DISCUSSION AND CONCLUSION 36
CHAPTER 5 – FUTURE DIRECTIONS 40
5.1 Long PM runs (Anton Machine) 40
5.2 Osh4 studies 41
List of Publications 42
List of Conference Presentations 43
CHAPTER 6 - REFERENCES 44

List of Figures

Figure 1- PM model.....1
Figure 2 - Chemical structure of lipids used in membrane models.....4
Figure 3 - Yeast secretory pathway.....9
Figure 4 - Periodic boundary conditions.....14
Figure 5 - Lipid composition, by headgroup, for each yeast membrane model.....19
Figure 6 - Surface area per lipid ($Å^2$).....23
Figure 7 – Average electron density profiles.....25
Figure 8 - Overall electron density profiles for yeast membranes.....27
Figure 9 - Sample calculation of bilayer thickness.....27
Figure 10 - S_{CD} parameters.....29
Figure 11 – S_{CD} parameters for the ER models 1 (top) and 2 (bottom).....30
Figure 12 - S_{CD} parameters for the TGN models 1 (top) and 2 (bottom).....31
Figure 13 - S_{CD} parameter for the PM models 1 (top) and 2 (bottom).....31
Figure 14 - S_{CD} parameters for the AVG-Yeast model.....32
Figure 15 – Lipid wobble.....32
Figure 16 - Correlation function c2(t).....33

Representations from all simulations were constructed with 'Visual Molecular Dynamics' (VMD) software (1), unless stated otherwise.

List of Tables

Table 1 - Model lipid types 20
Table 2 - Average surface area per lipid and compressibility modulus.....25
Table 3 – Bilayer thicknesses of yeast membranes 28
Table 4 – Relaxation times for the second carbon of glycerol correlation. 34
Table 5 – Relaxation times for the cross-chain correlation.....34

List of Abbreviations

CHOL	Cholesterol
DOPC	1,2-dioleoyl-*sn*-glycero-3-phosphocholine
DPPC	1,2-dipalmitoyl-*sn*-glycero-3-phosphocholine
DYPC	3-palmitoleoyl-2-palmitoleoyl-D-glycero-1-Phosphatidylcholine
DYPE	3-palmitoleoyl-2-palmitoleoyl-D-glycero-1-Phosphatidylethanolamine
EDP	Electron density profile
ER	Endoplasmic reticulum
ERG	Ergosterol
FA	Fatty acid
FF	Force field
GC	Gas Chromatography
HPLC	High performance liquid chromatography
L_d	Liquid disordered domain in membranes
L_o	Liquid ordered domain in membranes
LTP	Lipid transport protein
MD	Molecular dynamics
PA	Phosphatidic acid
PBC	Periodic boundary conditions
PC	Phosphatidylcholine
PE	Phosphatidylethanolamine
PI	Phosphatidylinositol
PM	Plasma membrane
PME	Particle mesh Ewald
POPA	3-palmitoyl-2-oleoyl-D-glycero-1-Phosphatidic acid
POPE	1-palmitoyl-2-oleoyl-*sn*-glycero-3-phosphoethanolamine
POPI	1-palmitoyl-2-pleoyl-inositol
POPS	3-palmitoyl-2-oleoyl-D-glycero-1-Phosphatidylserine
PS	Phosphatidylserine
PYPE	3-palmitoyl-2-palmitoleoyl-D-glycero-1-phosphatidylethanolamine
PYPI	1-palmitoyl-2-palmitoleoyl-sn-glycero-3-phosphoinositol
SA	Surface area per lipid
SANS	Small angle neutron scattering
SAXS	Small angle X-ray scattering
S_{CD}	Deuterium order parameters
SDP	Scattering density profiles
SM	Statistical mechanics
TGN	Trans Golgi network
TLC	Thin layer chromatography
VDW	van der Waals
YOPA	3-palmitoleoyl-2-oleoyl-D-glycero-1-phosphatidic acid
YOPC	3-palmitoleoyl-2-oleoyl-D-glycero-1-phosphatidylcholine
YOPE	3-palmitoleoyl-2-oleoyl-D-glycero-1-phosphatidylethanolamine
YOPS	3-palmitoleoyl-2-oleoyl-D-glycero-1-phosphatidylserine

CHAPTER 1 - BACKGROUND

1.1 Biological membranes

Membranes are essential for biological systems. They define the barrier between compartments within the cell as well as the boundary between itself and its surroundings (2, 3). Membranes are dynamic barriers formed by lipid bilayers that modify their organization to allow nutrients in and out of the cell; one of the model membranes used in this study is shown in Figure 1. The diversity of each membrane allows compartmentalization within the cell, critical for its survival. Membranes are used as energy storage compartments, and channels to communicate information between cells. The latest models describe the membrane as a patchy surface formed by a lipid bilayer with distributed proteins. The different regions in the bilayer have their own functionality, and must contain certain proteins at specific concentrations to properly function (4).

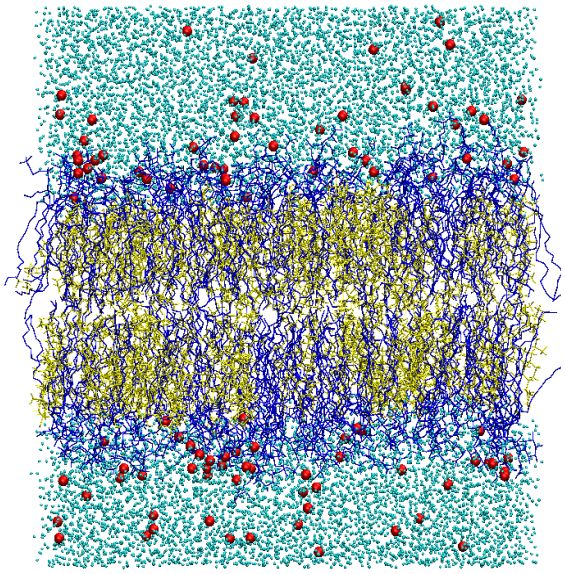

Figure 1- PM model
(blue: lipids; yellow: ergosterol; red: potassium ions). All figures were made using VMD software (1) unless indicated

1.1.1 Membrane Lipids

Membrane lipids are long amphiphilic molecules, i.e. have a hydrophobic tail and a hydrophilic head. They are used to store energy in the form of fatty acids and sterols in mammalian cells, but mainly as cell and organelle protectants in the case of single-cell

organisms like yeast. These lipids arrange in a bilayer structure, whose interior is a suitable hydrophobic core for transmembrane proteins (5, 6). The length and unsaturation degree of the lipid tails allow them to be versatile and able to adopt fluid or solid phases when forming the membrane bilayer structure. The current understanding of membrane dynamics shows lipids are free to move laterally in the membrane, enabling them to form distinct phases or domains. The adopted phase depends on the lipid structure; i.e. chain length and degree of saturation. The chemical structures and names of the biologically relevant lipids used in this research are shown in Figure 2. Membrane proteins are thought to impact these phase behaviors, forming lipids rafts throughout the membrane. Just like membrane proteins, membrane lipids distribution and concentration across the bilayer also affect the curvature and function of the membrane (2, 7).

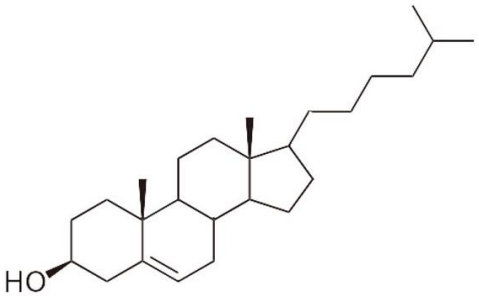

Cholesterol

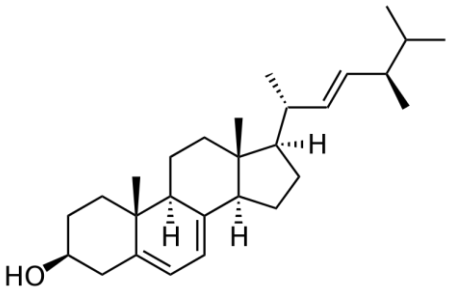

Ergosterol

POPA

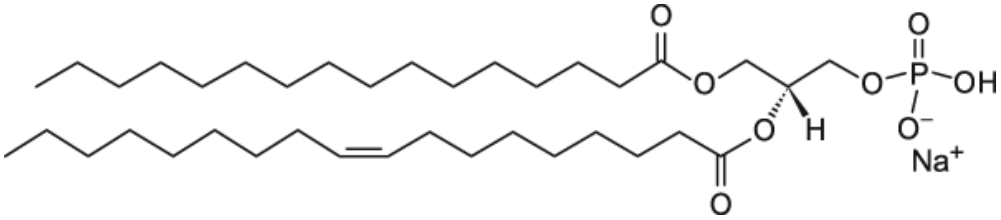

YOPA

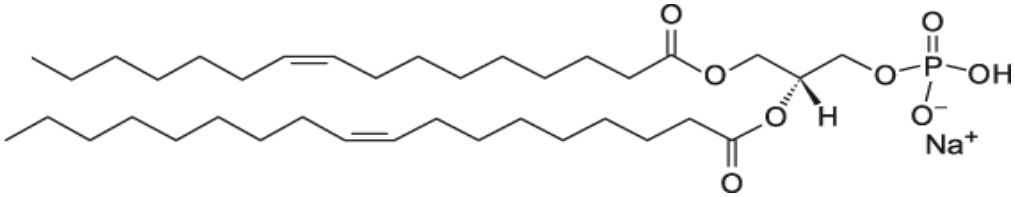

DOPC

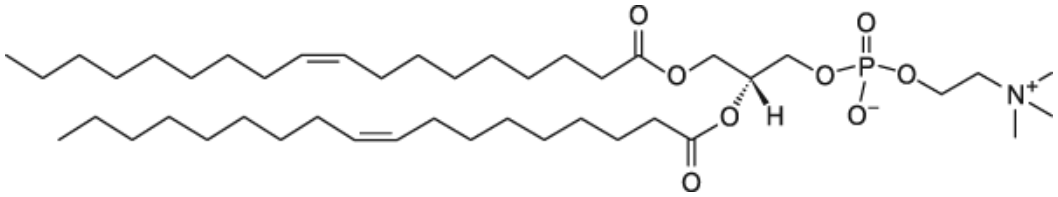

DPPC

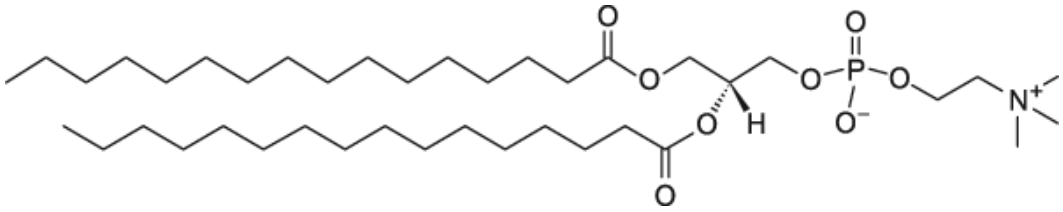

DYPC

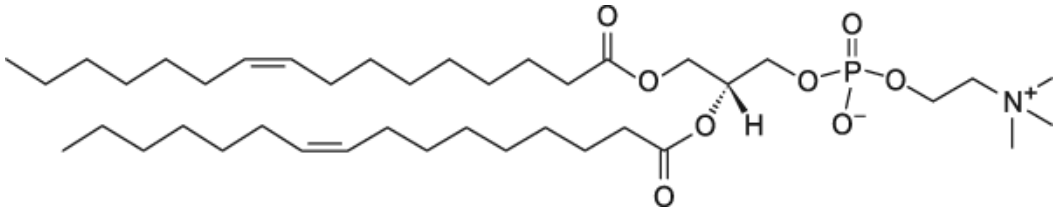

YOPC

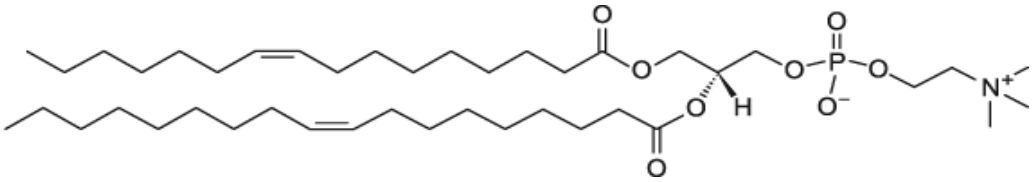

DYPE

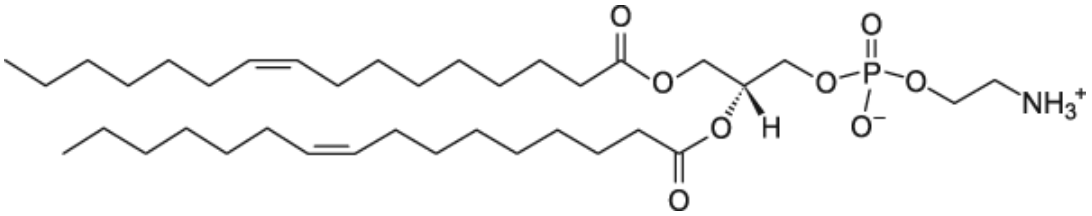

POPE

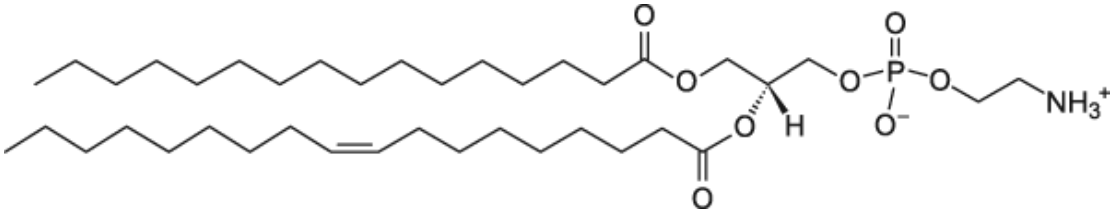

PYPE

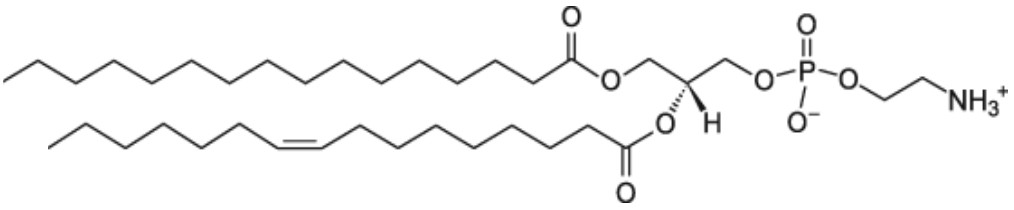

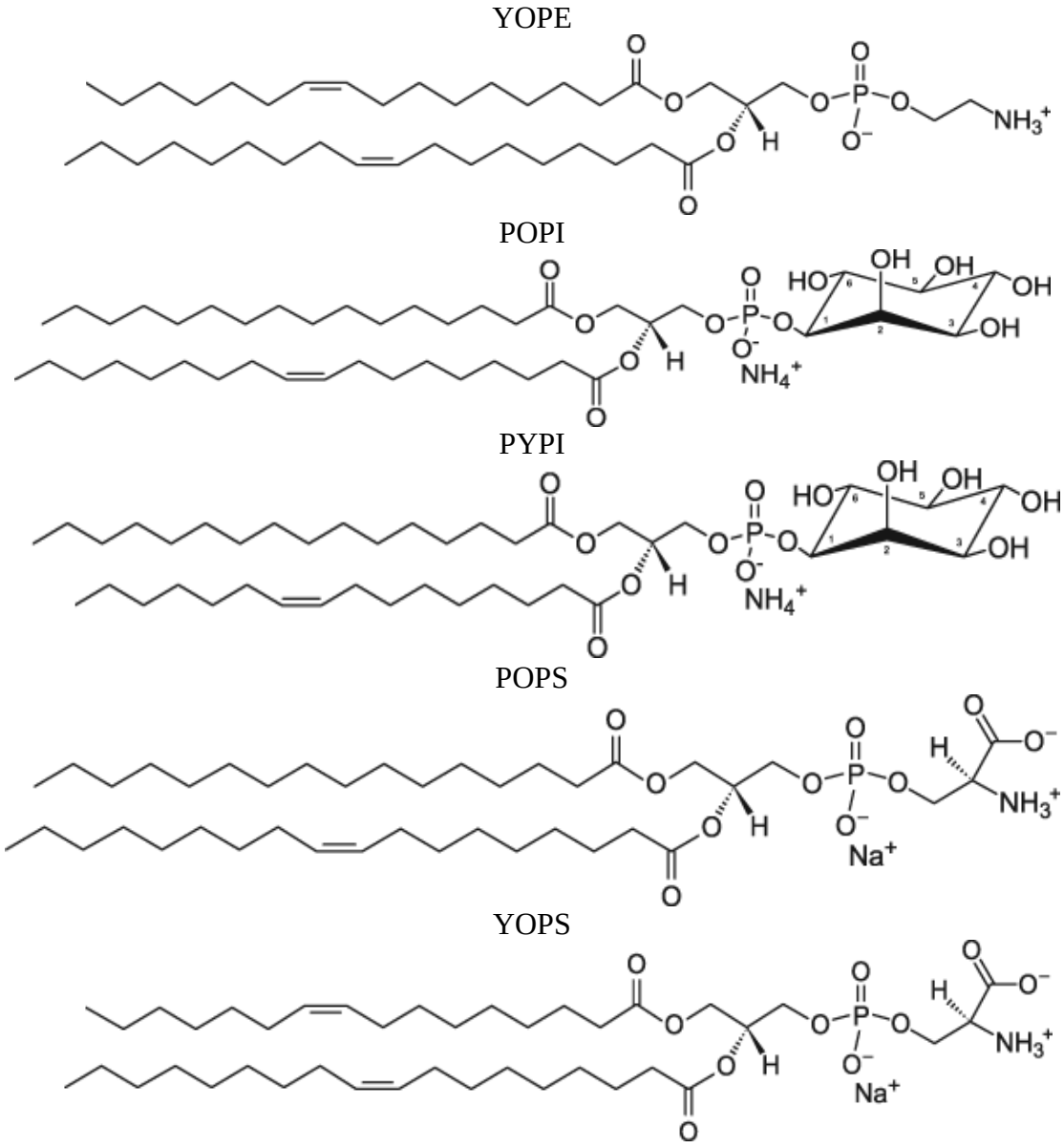

Figure 2 - Chemical structure of lipids used in membrane models

3-palmitoyl-2-oleoyl-D-glycero-1-phosphatidic acid (POPA); 3-palmitoleoyl-2-oleoyl-D-glycero-1-phosphatidic acid (YOPA); 1,2-Dioleoyl-*sn*-glycero-3-phosphocholine (DOPC); 1,2-dipalmitoyl-*sn*-glycero-3-phosphocholine (DPPC); 3-palmitoleoyl-2-palmitoleoyl-D-glycero-1-phosphatidylcholine (DYPC); 3-palmitoleoyl-2-oleoyl-D-glycero-1-phosphatidylcholine (YOPC); 3-palmitoleoyl-2-palmitoleoyl-D-glycero-1-phosphatidylethanolamine (DYPE); 1-palmitoyl-2-oleoyl-*sn*-glycero-3-phosphoethanolamine (POPE); 3-palmitoyl-2-palmitoleoyl-D-glycero-1-phosphatidylethanolamine (PYPE); 3-palmitoleoyl-2-oleoyl-D-glycero-1-phosphatidylethanolamine (YOPE); 1-palmitoyl-2-oleoyl-inositol (POPI); 1-palmitoyl-2-palmitoleoyl-sn-glycero-3-phosphoinositol (PYPI); 3-palmitoyl-2-oleoyl-D-glycero-1-phosphatidylserine (POPS); 3-palmitoleoyl-2-oleoyl-D-glycero-1-phosphatidylserine (YOPS).

The diversity of lipids varies for different organisms; in yeast, the organism of study in this work, most of the structural lipids are the glycerophospholipids. Among them,

phosphatidic acid (PA), phosphatidylcholine (PC), phosphatidylethanolamine (PE), phosphatidylserine (PS), and phosphatidylinositol (PI) lipids are the most common. However, sterols are by far the predominant non-polar lipids in biological membranes; ergosterol (ERG) is the major sterol representative in yeast cells. Lipid headgroups are neutral, charged, or have ring structures; these influence largely the dynamics of the membrane as well as the activity of membrane proteins and surface potential of the membrane (8). Sphingolipids, mainly structural lipids of mammalian cells, are also present and play important roles in other eukaryotic cells like yeast, but are not in the scope of this work (2, 9) due to the lack of accurate simulation parameters at the start of this study. Future directions including this type of lipids are discussed in the last chapter of this work.

Given the important roles of lipids in the stability of the cell, complex mechanisms take place to maintain their level in the different organelle membranes. Current methods to study the lipid profile of a cell are thin layer chromatography (TLC), gas chromatography (GC), and high performance liquid chromatography (HPLC). Nonetheless, even advanced methods such as shotgun lipidomics platform do not provide detailed information on the regulatory functions of lipids (9). Cell signaling and sensing, as influenced by lipid composition, have not yet been fully understood. Lipid transport and assembly onto organelle membranes is an expanding area of research. The influence of lipid composition as well as lipid synthesis and trafficking on protein folding and activity are also under current examination (6, 10). The goal of the present work is to determine the effect of lipid composition in the structural, mechanical and dynamical properties of yeast membrane models. More details on the role of lipids in different organelles of yeast cells is given in Chapter 2.

1.1.2 Membrane proteins

Proteins are essential in all biological processes. They act as catalysts (enzymes), transporters, storage units, mechanical support, transmitters, or controllers of growth and differentiation. The primary structure of a protein is determined by its sequence of amino acids – basic structural units. Proteins range from small peptides formed by tens of amino acids, to large complexes formed by hundreds of amino acids. These can be polar, non-polar, hydrophobic, neutral, or charged molecules that determine the secondary structure of proteins according to their sequencing order. Secondary structures include α-helices, β-sheets, and loops or random coils. Large proteins may have several secondary structures in their backbone, and their configuration in space forms the tertiary structure of the protein, which may vary according to its surroundings and activate or deactivate the protein. The stability of a protein comes largely from van der Waals and hydrogen-bond interactions in its structure (11).

Transport of molecules across the membrane is an important process in cells and occurs through proteins, which may act as channels to let nutrients in or out the cell. Membrane channels exhibit high selectivity, conductivity, and sensitivity. For example, the channels for water, gases, and small alcohols are called aquaporins; and potassium is transported through potassium channels (12). Protein distribution in the bilayer is not random; in addition to determining the functions of the membrane, transmembrane proteins also influence the curvature of the bilayer as well as the membrane's electrostatic interactions with its surroundings (2). Membrane proteins can also have peripheral domains that bind to the surface of the bilayer; these proteins can act as enzymes or lipid transporters. Lipid-transport proteins (LTPs) provide an alternative to vesicular transport in shuttling lipid and

small molecules between organelles (13). Membrane lipids highly influence the function of the membrane and the binding, activation, and signaling of proteins in and around the bilayer.

1.1.3 Sterols

Biological membranes are also hosts to small molecules such as ions, and smaller lipids like sterols that contribute to the proper function and mechanical properties of the cell. Cholesterol (Figure 2) is widely known to play a very important role as regulator of cell properties in mammalian cells (7, 14). Ergosterol (Figure 2), its homologue in fungal cells like yeast, is also crucial for cell survival. Ergosterol and cholesterol only differ in the number of double bonds in the sterol tail and center six-membered ring, but they both behave similarly (15). Sterols influence the fluidity and order of the bilayer, and can also affect the cell's response to disease. At high concentrations sterols induce lipid domains, separating the membrane into liquid-order (L_o) sterol-rich and liquid-disordered (L_d) sterol-poor phases. This phase separation gives rise to important membrane dynamics and changes in its mechanical properties. Such changes are important in determining how the cell responds to its environment. Sterol flux within the cell, along with lipid reorganization, ensures each organelle maintains viable concentration of its lipids. Besides sterol flux and composition, intrinsic membrane curvature is also responsible for lipid reorganization within the bilayer (2, 14, 16, 17).

Sterol levels in the plasma membrane are critical for cell operations; though synthesized in the endoplasmic reticulum, sterols are unevenly distributed in all cellular organelles until they reach the plasma membrane. Sterol levels seem to be tightly controlled in the cell to

prevent any dysfunction. In yeast, sterols are transported by vesicles as well as LTPs. Common LTPs in yeast are members of the oxysterol binding homologue protein family (Osh). Besides sterols, the Osh proteins also transport other lipids like PI4P, and the specific role of each protein is currently under study. Deletion of the seven members of this family (Osh1-Osh7) results in cell death (10, 18).

1.2 Yeast membranes

Saccharomyces cerevisiae is a very common reference organism in modern biology. Its complete genome sequence is known, and in the past 20 years several studies were made to expand our understanding of its diverse cellular processes. *S. cerevisiae* is the organism better understood among eukaryotes in terms of its genetics and metabolism, but studies on its lipidome are still limited. Most eukaryotes have well-conserved mechanisms, and their gene homology with yeast is high (6). Experimentally, yeast is a favorable model because it is simple to grow and manipulate versus mammalian cells, and it conserves most of the fundamental metabolic pathways against mammals. Finally, the diversity of lipids in yeast ascends to a few hundred, while mammalian cells have over thousands and their characterization for cell homeostasis would be extremely time consuming (10). The scope of this work focuses on three yeast organelles involved in the secretory pathway of the cell, its route for degradation and recycling among others (see figure 3).

1.2.1 Endoplasmic Reticulum (ER)

The ER is a dynamic network of sheets and tubules that expands from the nucleus to the plasma membrane. Proteins and lipids are mainly synthesized in this organelle, and it is also the starting point of the secretory pathway (2). However, important lipid synthesis also

takes places in the Golgi complex, plasma membrane, and mitochondria (13). The ER closely interacts with most organelles in the cell and has the most fluid membrane. Interaction sites allow for non-vesicular transport of lipids and calcium signaling. Correct dynamics and morphology must be maintained in this organelle to prevent cell malfunction. Changes in the ER lipid or protein composition alter the metabolism of the cell by affecting lipid biogenesis (19). Transmembrane proteins are very important in modulating the shape of the ER, these have been proposed to form wedge-like structures in the outer leaflet of the bilayer, inducing positive curvature in the membrane which in turn induces membrane deformation relevant for cellular processes (20, 21).

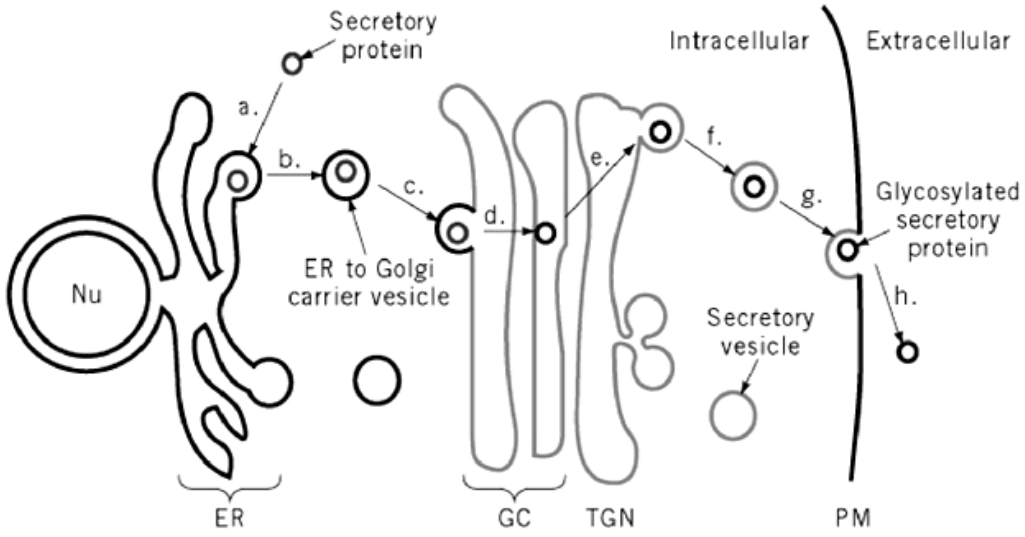

Figure 3 - Yeast secretory pathway
Diagram showing vesicular transport of degraded/recycled material to the exterior of the cell.
(*http://what-when-how.com/molecular-biology/protein-secretion-molecular-biology/*)

1.2.2 Trans-Golgi Network (TGN)

The TGN is a sorting station for lipids and proteins in the secretory pathway, and storing area for some biochemical molecules before they are delivered to their final location. This membrane resists many of fluxes coming to and from the ER and plasma membranes, so

its steady state cisternal-like arrangement is temporary. Malfunction of the TGN results in interference of protein modification, sorting, and delivery, affecting a wide variety of cellular processes. Current studies show lipid metabolism is closely linked to TGN function and resiliency. PI lipids are involved in the regulation of membrane trafficking and secretory regulation of the Golgi system. Sterols and LTPs are also among important contributors to proper Golgi function. In addition, the Golgi apparatus was shown to be a major producer of sphingolipids (9, 22, 23).

1.2.3 Plasma Membrane (PM)

The PM is the outermost membrane of the cell, it is also the most rigid bilayer. It is the final membrane where lipids arrive, and its composition and health are dependent on a functional secretory pathway. Sterol composition in this membrane is critical to ensure its proper rigidity and allow cell growth. The high sterol content in the PM gives rise to sterol-rich microdomains, very important for exchange dynamics and diffusion of lipids in the cell (7). In addition, studies in the past two years have found sterol-free microdomains (gel phase) that are rich in sphingolipids in the PM, but conclusive findings are yet to be published (24). The PM composition is very different from the other organelles, containing high concentrations of sphingolipids and ceramides. Most of the sphingolipids in yeast are located at the PM, and they constitute about 30% of the total lipid content in this membrane. Lipids are delivered to the PM by vesicular transport or LTPs from the ER and TGN. This membrane is largely populated by transmembrane proteins, which are often restrained by their association with other proteins to allow a fully functional membrane. The PM is also very sensitive to changes in nutrition and environment (8, 25).

1.3 Molecular Dynamics (MD) Simulations

Cellular processes can take place over short timescales; MD simulations facilitate their study and can be helpful in the selection of experimental targets. This simulation technique is deterministic, based on statistical mechanics and empirical energy functions. The basic idea is to model the interactions within a system based on forces acting on its atoms. Given a set of coordinates for a system, initial velocities are randomly generated for each atom using equation 1, the Maxwell-Boltzmann distribution at a given temperature, where v_α is the α component of the velocity at time *t* (26). Newton's laws of motion are determined for each atom based on its velocity (*v*) and forces acting over it to generate simulation trajectories that specify its position (*r*) over the course of time. The integration of Newton's equations results in equations 2 and 3 for the position and velocity of each atom in the system using, for example, the Verlet algorithm. Initial coordinates for a system are based on the chemical structure of a molecule obtained from experimental data; crystallographic structures are used in the case of proteins (27).

$$\langle v_\alpha^2 \rangle = \left(\sum_{i=1}^{N} {mv_{\alpha,i}^2(t)}/{N_t} \right)/m \qquad \textbf{(1)}$$

$$r(t+\Delta t) = 2r(t) - r(t-\Delta t) + \left({f(t)}/{m}\right)\Delta t^2 \qquad \textbf{(2)}$$

$$v(t) = {\{r(t+\Delta t) - r(t-\Delta t)\}}/{2\Delta t} + O(\Delta t^2) \qquad \textbf{(3)}$$

The first stage of MD simulation proceeds until the properties of the system, like total energy and temperature, do not vary over time, i.e. the system is equilibrated. All properties of simulation experiments are calculated after the system has run a production phase, where a trajectory is generated at the desired temperature, pressure, or volume (extended details

in the next chapter). The desired property must be expressed in terms of the position and momenta of each atom in the system. Computational results must be averaged over replica experiments to obtain statistically relevant results (26).

MD techniques have evolved in the past 50 years to represent atomic models more accurately. A very simple model represents the atoms in a system as hard-spheres. The hard-sphere potential represents all atoms with the same sphere size, accounts for fully elastic collision between atoms, and assumes the atoms move in straight lines after collision with another sphere. On the other hand, the square-well potential sets two cut-off values; the interaction energy is zero above the higher limit, infinite below the lowest limit, and a set value in between. Although limited, this model provided the first insights into microscopic properties of fluids in MD. More complex models use a continuous potential that updates the forces acting on an atom every time it changes position. In this case, the integration of the laws of motion is made by finite difference method. To avoid large errors due to fast motions in a molecule, the integration time step is commonly set to 1-5fs depending on the molecule of study (26).

1.3.1 Force Fields

MD uses force fields (FF) to describe inter- and intramolecular forces that govern the system of study. Forces acting on the system are evaluated through a potential energy function, $V(\hat{R})$, where $\hat{R}$ stands for the position of atoms in the system see (equation 4). A FF is divided in terms that account for bonded and non-bonded terms, attractive and repulsive forces, angles bending, torsional and rotational energies. If a system only has simpler molecules, the FF is reduced in complexity (26). Intramolecular forces are

evaluated looking at the bond and angle energy terms in the energy function. Non-bonded interactions specify the relationship of every atom in the system with its far-neighboring atoms. These are accounted for in the attraction and repulsive components of the van der Waals (VDW) potential, evaluated by a 12-6 Lenard-Jones potential with cut-off values set by the user (27).

$$V(\hat{R}) = \sum_{bonds} K_b (b - b_0)^2 + \sum_{angles} K_\theta (\theta - \theta_0)^2 + \sum_{cross\mathrm{UB}} K_{UB} \left(r_{1,3} - r_{1,3}^0\right)^2 + \sum_{improper} K_{im} (1 - \cos(2\phi)) + \sum_{dihedrals} \left[\sum_j K_{\varphi,j} (1 + \cos(n_j \varphi - \delta_j)) \right] + \sum_{\substack{nonbonded \\ pairs i,j}} \varepsilon_{ij} \left[\left(\frac{R_{\min,ij}}{r_{ij}} \right)^{12} - \left(\frac{R_{\min,ij}}{r_{ij}} \right)^{6} \right] + \sum_{\substack{nonbonded \\ pairs i,j}} \frac{q_i q_j}{\varepsilon_D r_{ij}} \quad \textbf{(4)}$$

An important characteristic of FFs is the parameters used to determine the energy contributions of the different terms in the empirical function. The set of parameters is unique to the FF of choice and determine its accuracy. FF parameters are set to reproduced desired properties of different chemical structures; the choice of FF is left to the user according to the study target (26). This work used the CHARMM36 (C36) FF that takes on the general form in equation 4; our simulations used the most updated parameters for PI lipids (28, 29). VDW and electrostatics were computed using a force-based switching function from 8 to12 Å. All simulations were run using periodic boundary conditions (PBC) that evaluate electrostatic interactions using Particle Mesh Ewald (PME). Simple PBC use the central box of a simulation, for which all coordinates are defined, and 26 images of it on all faces to prevent erroneous calculation due to the interaction of atoms with the walls of the system (30). As an atom moves out of the central box, its image appears on the opposite side as it is moving outside from the neighboring image (see figure 4).

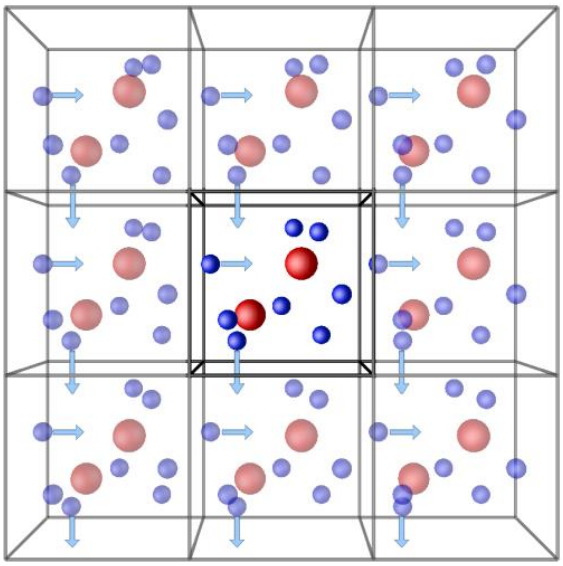

Figure 4 - Periodic boundary conditions (http://isaacs.sourceforge.net/phys/pbc.html)

The all-atom MD simulations of model membranes in this thesis were run using CHARMM and NAMD (31, 32) software packages; all systems were neutral to meet the requirements of NAMD for PME. C36 FF allows heterogeneous MD simulation runs in the isobaric-isothermal (NPT) ensemble with no surface tension, and reproduces more accurately experimental properties such as deuterium order parameters (S_{CD}) near the membrane-water interface and lipid rotation rates. Other simulation studies of membrane models done using the C36 FF render results in agreement with experimental data, and provided useful insights on membrane properties similar to those of interest in this work (15, 33).

1.3.2 Temperature and Pressure control in MD

MD simulations are based on statistical mechanics (SM); this approach gives a molecular interpretation and prediction of macroscopic properties of a system. A macroscopic property results from the average value of that property for the weighted probability of each microstate. A microstate is a system of particles with a total energy based on the single energies of the atoms forming that system. The simulation of a closed system at constant number of molecules (N), volume (V), and temperature (T), is said to be using the NVT (Canonical) ensemble (34, 35). The use of other ensembles may be more appropriate depending upon the properties that want to be calculated. However, the NPT ensemble is

one of the most common in MD, and all thermodynamic properties are derived from the Gibbs energy (G) of the system (26, 34).

The temperature of a system is related to its average kinetic energy over time. CHARMM uses an accurate method developed by Nosé in 1984, and further improved by Hoover; now known as the Nosé-Hoover thermostat. This thermostat uses a thermal bath as key component of the system, and extended Lagrangian methods that contain artificial coordinates and velocities for the system. The temperature is kept constant in the real system by calculating the position of each atom times a parameter that determines the coupling between the real and extended systems. NAMD runs utilize Langevin dynamics to maintain the temperature constant throughout simulation (26, 27).

For constant pressure control, the volume is the dynamic variable and its equation of motion is added to the set of equations for the simulation. CHARMM controls the pressure using the Nosé-Hoover piston, allowing the cell box size to change isotropically. In NAMD, the pressure is controlled using the Langevin piston Nosé-Hoover method, which couples the piston controls to a temperature bath controlled by Langevin dynamics and compatible with the pressure control in CHARMM (32, 36, 37).

CHAPTER2 - METHODS

2.1 Building and Equilibration techniques

The systems for our MD simulations were constructed using the *Membrane Builder* of CHARMM-GUI (www.charmm-gui.org), an automated graphical user interface to build heterogeneous systems (15, 38, 39). CHARMM-GUI has a library of over 200 lipids classified by headgroup structures and sterols (40). The number of lipids per leaflet, or their relative ratio, is entered into the builder along with the level of hydration for the system, i.e. the number of water molecules per lipid, or water thickness above and below the bilayer. The system is built based on estimates for the area per lipid for each component; this estimate is very important to ensure enough space between molecules in their initial position to avoid clashes or ring penetration issues. Lipid orientations in the bilayer are randomly chosen from a set of 1000 orientations for each molecule; the bilayer order and structure is therefore unbiased. Subsequent building steps include setting a preferred temperature, thermodynamic ensemble, and the addition of ions to render a neutral system, or as specified by the user.

The simulation box undergoes a short equilibration and check for ring penetration or bond breakage occurrences before the PDB, PSF, topology, parameter, restraint, and equilibration input files are output for the user. The *Membrane Builder* provides the user with CHARMM and NAMD input scripts that can be modified if needed. Typical equilibration is achieved in a series of 6 consecutive steps, the first two run using NVT dynamics (constant number of molecules, volume, and temperature). The remaining four steps use the NPT ensemble gradually decreasing restraint force constants that prevent FA

double bonds from changing its *cis*/*trans* conformation, keep PI lipids in the chair conformation, maintain C2 chirality in each lipid, and hold the lipid head groups in position along the z-axis (40).

2.2 Systems of study

The current developments in all-atom simulations and computational capabilities allow us to study cellular processes in different organisms. However, currently available models are not diverse enough to expand the knowledge in membrane signaling and trafficking in cells, or protein-lipid interactions with accurate precision. Seven membrane models were developed to study the impact of lipid composition in the membrane properties of organelles involved in the secretory pathway of yeast cells. The first model is a replicate of a simple model for yeast studied in our lab based on the overall lipid composition (15). More complex models were built for the PM, ER, and TGN based on experimental data (9, 25, 41, 42). Comparison between the simple and more complex models can be found in Sections 3 of this work.

2.2.1 Average Yeast Model (AVG-Yeast)

This model is based on a previous study by Jo *et al.* to explain the capabilities of the *Membrane Builder* in CHARMM-GUI to construct heterogeneous lipid bilayers (15). The model contained the most representative lipids of yeast cells; however, their relative concentrations are average values between cell organelles taken from an experimental study (41). The Jo *et al.* study explored the effect of cholesterol concentration on membrane properties, among others. The present work will use this model as a control system to show the importance of accurate model representation for specific organelles in yeast. Given the

moderate concentration of sterol in this model, the results for the PM model are expected to match AVG-Yeast better than the ER or TGN models due to its high sterol composition. In addition, discrepancies in the calculated properties will arise from the structural and unsaturation differences between cholesterol (the sterol in AVG-Yeast) and ergosterol in the new models. The AVG-Yeast model, as the rest of the system studied in this work, was simulated using the C36 FF to be consistent.

The lipid composition for AVG-yeast was taken from Daum *et al.* experimental assays (41). The yeast strain used as basis for this model is CPR-Δ1, and although sphingolipids and PI are analyzed in the experimental tests of this strain, they were not included in the theoretical model as parameters were not available when AVG-Yeast was first developed. The most representative fatty acids were experimentally determined to be palmitoleic (C16:1) and oleic (C18:1) with 62.5% and 26.1% respectively. Small percentages of palmitic (C16:0) and stearic (C18:0) were also present. The theoretical model was design with 45.5 unsaturation fraction, using simple phospholipids to represent this strain. Figure 5 shows the lipid composition of all the models used in this study according to lipid headgroups, specific lipid types are listed in Table 1 in the next section. Note the lipid types based on headgroup diversity have the same composition for both models of the organelles of interest. The difference between the two models for each organelle comes from the unsaturation degree.

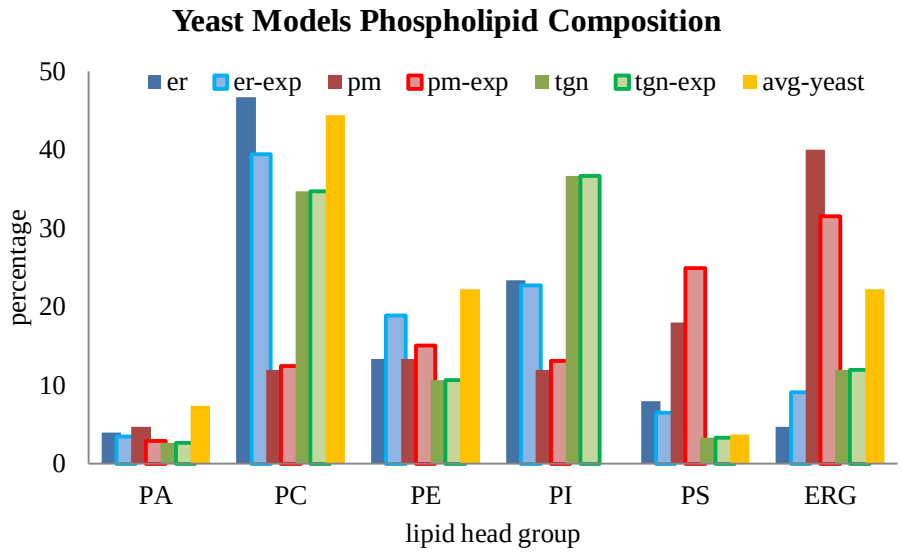

Figure 5 - Lipid composition (by headgroup); *"*-exp"* refer to available experimental data. The sterol used in avg-yeast was Cholesterol, but its composition is shown under ERG in this graph

2.2.2 Complex Models

As mentioned previously, lipid concentration and organization in a given bilayer is critical to its function and overall cell survival. In fact, each organelle has a specific lipid pattern that serves as a signature of healthy or sick cell condition (43). To successfully study membrane properties and processes using MD simulations it is necessary to accurately account for the lipid composition characteristic to the organelle of interest. Two models were developed for each organelle of study, varying in lipid concentration, diversity, and unsaturation degree as listed on Table 1. PI lipids were not yet in the *Membrane Builder* library at the moment of building the first ER and PM models, and missing coordinates where incorporated manually using CHARMM scripts.

The most representative sterol in the PM of yeast is ERG, while the most common fatty acids (FA) in this organelle are palmitic (16:0) and oleic (18:1) acids. These results in a low ratio of unsaturated to saturated fatty acids compared to other organelles (25). PS lipids

are abundant in the PM, but may be triggers for apoptosis, i.e. programmed cell death, if not properly regulated. PS and ERG increase in parallel concentration along the secretory pathway, so that the ER contains the least concentration of these lipids (43). Corresponding to these values, ERG, POPE, POPI, and POPS lipids were included in larger amounts in the PM models built for this study.

Table 1 - Model lipid types by headgroup and unsaturation content of the *sn2-sn1* tails. The *sn-2* FA is the one attached to the oxygen atom on the second carbon of glycerol

Lipid		**Unsaturation *(sn2-sn1)***	**er1**	**er2**	**pm1**	**pm2**	**tgn1**	**tgn2**	**avg-yeast**
sterol	ERG		7	7	60	60	18	18	
	CHOL								30
PA	POPA	18:1-16:0					4	0	10
	YOPA	18:1-16:1	6	6	7	7		4	
PC	DYPC	16:1-16:1	42	42	12	18	29	40	
	YOPC	18:1-16:1	28	28	6		23	12	
	DPPC	16:0-16:0							10
	DOPC	18:1-18:1							50
PE	DYPE	16:1-16:1	10	10			6	8	
	POPE	18:1-16:0			9	20			30
	PYPE	16:1-16:0			5		4		
	YOPE	18:1-16:1	10	10	6		6	8	
PI	POPI	18:1-16:0	21	21	10	18	27	13	
	PYPI	16:1-16:0	14	14	8		28	42	
PS	POPS	18:1-16:0	6	12	21	27	5		5
	YOPS	18:1-16:1	6		6			5	
lipids per leaflet			*150*	*150*	*150*	*150*	*150*	*150*	*135*
total # of atoms			*74.3K*	*65.1K*	*71.6K*	*59.9K*	*88.4K*	*88.2K*	*72.6K*

On the other hand, the ER models used in this study were built to reflect the more fluid structure of this organelle (43). This model contains the least amount of ERG, but the highest concentration of PC lipids. Other characteristic ER lipids, included in the models, are PIs and PEs. The only difference between the two models built for this study is the

unsaturation degree of the PS lipids; one model uses oleic (18:1) and palmitoleic acid (16:1), while the other one substitutes the latter for palmitic acid (16:0).

Along with the ER, the TGN also plays an important role in lipid biogenesis, mutation, and further transportation of lipids to the PM or other storage locations. Klemm *et al.* published a comprehensive study in 2009 (9), from where the model lipids for this study were selected. From the FA analysis, it was determined oleic (18:1) and palmitoleic (16:1) acids are the by far the most representative FA in the TGN. The PI lipids were the only ones with a different FA distribution, where palmitic acid (16:0) was the dominant FA. Based on these findings and specific percentages for lipid headgroups, the PC and PI lipids were selected as the dominant phospholipids for the membrane models along with a moderate concentration of ERG.

Lipid composition has also a particular signature in the inner and outer leaflet of membrane bilayers; especially in the PM, where sphingolipids play an important role in protein-bilayer interaction (6, 24). Although this is not accounted in the models presented in this work, it has been shown of importance for cell signaling processes (19, 42).

2.3 MD simulations settings

NAMD and CHARMM packages were used to run 200ns trajectories for each system. All simulations followed the six-step CHARMM-GUI protocol (15, 39) before running the production runs, a short NVT equilibration followed by NPT dynamics on CHARMM using C36FF and the TIP3P model for water (44). The production run of each system was run on NAMD with a 2fs time-step using the SHAKE algorithm to constraint hydrogen atoms (45). Van der Waals interactions were calculated using a Lennard-Jones force-

switching function over 8 to 12 Å (46), and the Particle Mesh Ewald method was used to account for long range electrostatics (47). Constant temperature (303.15K) and pressure (1bar) during the 225-ps CHARMM equilibration were achieved and controlled using a Hoover thermostat (48) and Nosé-Hoover piston (49) respectively. The 200-ns trajectories on NAMD (NPT dynamics) maintained the same temperature and pressure using a Langevin piston (36).

CHAPTER 3 - RESULTS AND DISCUSSION

A common equilibration metric for lipid bilayer simulations is stability in the lateral surface area. The ER and TGN membranes reached equilibrium after 25ns, shown by plateau of the average surface area per lipid (SA) on Figure 6. The plateau is especially noticeable on the PM membranes and AVG-yeast, which took longer simulation time to equilibrate – nearly 40 ns, and more than 50ns for PM2 – due to their high sterol content. Membrane properties in this thesis were calculated from the last 50ns of equilibrium data, unless stated otherwise. The reported results are the average values of each property over three replicate runs for each system.

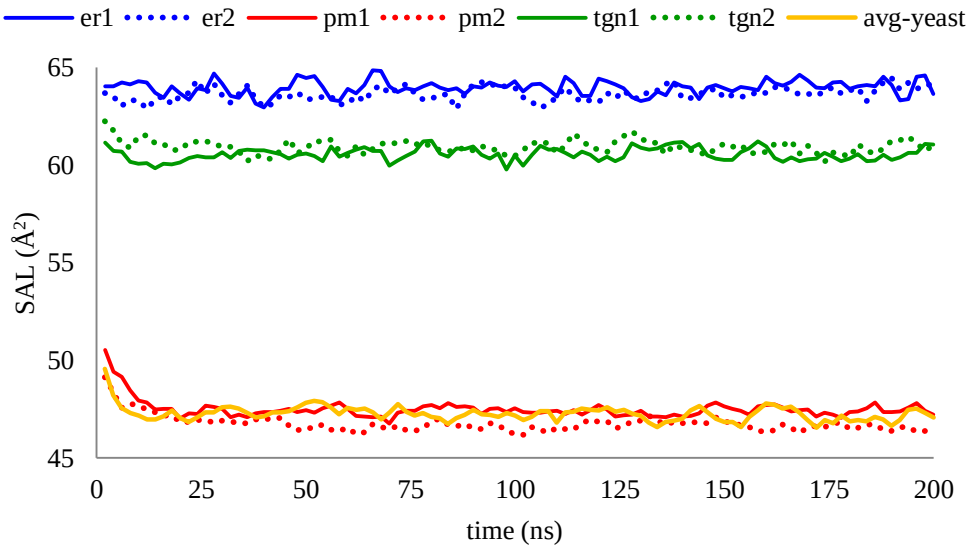

Figure 6 - Surface area per lipid ($Å^2$)

3.1 SA per lipid and Compressibility modulus (K_A)

As mentioned before, the surface area (SA) of the system gives us an idea of when the system reaches thermodynamic equilibrium, i.e. the temperature, volume, and total energy

of the system oscillate over an average constant value. Using the SA data the compressibility modulus is calculated directly using equation 5,

$$K_A = k_B T * {A_L}\Big/{\sigma^2_{A_L}} \qquad \textbf{(5)}$$

where k_B is the Boltzmann constant, A_L is the SA, and σ_A^2 its variance. K_A is a measure of a membrane stiffness, or resistance to uniform compression. Table 2 summarizes the results for the overall SA and K_A for each membrane. It is easy to see from these values, as well as Figure 6, the PM and AVG-yeast models have a lower surface area (46.76-47.42Å), but higher K_A values when compared to the other membranes. This occurs due to the presence of ERG, or cholesterol (CHOL) in the case of AVG-yeast. Sterols position themselves in between other lipid tails, creating a more ordered environment and a bulkier more rigid bilayer. Is interesting to note, however, that PM1, PM2, and AVG-yeast membranes have very different K_A values despite their similar SA.

PM1 and PM2 have the same headgroup diversity, but the degree of unsaturation for these models is 0.71 and 0.64, respectively. In other words, there are more unsaturated FA tails in the lipids of PM1, which introduce disorder in the bilayer as their conformation has kinks at the location of double bonds. Since PM2 has a more saturated environment than PM1, one would expect its K_A to be also higher than that of PM1; however, the results show statistical difference between the two. AVG-yeast, with the lowest K_A among the three (0.34±0.04 N/m), has a similar unsaturated fraction to PM2, but its sterol composition is 22.2%, a little more than half the percentage of sterol in the PM membranes (40%). Studies show CHOL has a higher influence in membrane order and fluidity compared to ERG (50); despite this, the lower value in K_A is expected in the AVG-yeast model because the sterol

content is not as high as that of the PM membranes, thus the bilayer is more fluid than the PMs. In addition, the average length of AVG-yeast (28.7) is smaller than PM2 (33.4), i.e. its total average number of carbons for each lipid (counting both FA tails) is less than PM2. The results are consistent with past studies (51, 52) that show smaller saturated FA chain lengths result in more ordered (fluid) bilayer structures. A more robust comparison on the effects of CHOL versus ERG could be made if the membranes had the same sterol composition, but that is out of the scope of this work.

Table 2 - Average surface area per lipid and compressibility modulus. Values are reported with their respective standard error.

model	SA/lipid (Å^2)	K_A (N/m)
er1	63.99 ± 0.38	0.29 ± 0.02
er2	63.65 ± 0.36	0.28 ± 0.02
tgn1	60.56 ± 0.36	0.28 ± 0.06
tgn2	60.95 ± 0.36	0.27 ± 0.02
pm1	47.42 ± 0.25	0.57 ± 0.06
pm2	46.76 ± 0.30	0.47 ± 0.08
avg-yeast	47.27 ± 0.32	0.34 ± 0.04

3.2 Electron density profiles (EDP)

The structure of biological lipid membranes is a very important topic of study; however, it is difficult to precisely determine atom positions due to thermal fluctuations. Bilayer structures have been studied using statistical averages

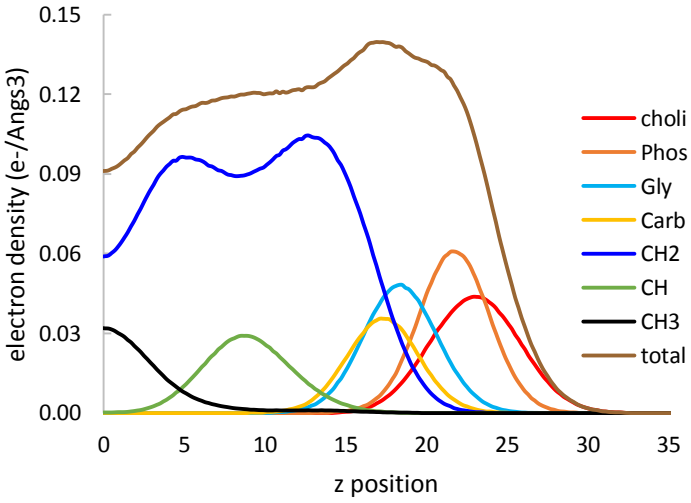

Figure 7 – Average electron density profiles DOPC in AVG-yeast showing separate lipid components.

based on neutron and X-ray scattering experiments. Small angle neutron scattering (SANS) is used generally to locate the position of the glycerol group in lipids, and small angle X-ray scattering (SAXS) is commonly used to locate the phosphate group (53, 54). These scattering density profiles (SDP) measure the electron density of lipids in a bilayer, which can also be computed from MD simulation data. Electron density profiles (EDPs) from simulation data are used to estimate bilayer thickness, which can be directly compared to experimental data, if available.

The EDP plots in this work were generated using SIMtoEXP software package and following the procedure of Kučerka *et al.* (55). The equilibrated data from each simulation was used to calculate the number of electrons per volume of each atom in the system, and then combined to get the EDP of a particular component as defined by the user. The location of different chemical groups or lipid components with respect to the z-axis can be easily located in an EDP. For example, the methyl group EDP of DOPC from AVG-yeast, shown in Figure 7, has a peak at the center of the bilayer, denoted by z=0. The carbons in the tails with single (CH2) or double bonds (CH), shown in blue and green respectively, are within the total EDP (brown curve) and in the middle section of the leaflet as expected. Hydrophilic components, such as the phosphate group (orange) and headgroup (red) EDPs have peaks towards the side of the leaflet in contact with water.

The EDPs for each membrane were used to determine the head-to-head distance between the lipid phosphates on each leaflet (D_{HH}), the Luzzati thickness (overall bilayer thickness) of the bilayer (D_B), and its hydrocarbon region or core ($2D_C$). Figure 8 shows the overall EDPs for each system, calculated by adding the total EDPs for each lipid in the systems; D_{HH} was estimated from the peak values of each curve in this figure. D_B and $2D_C$ were

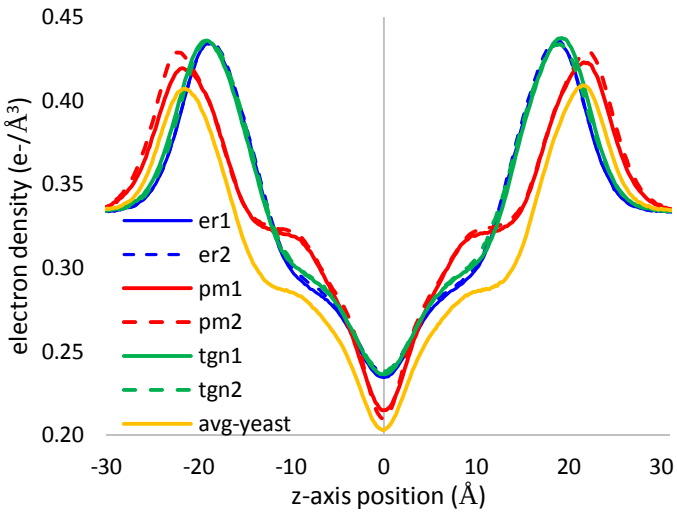

Figure 8 - Overall electron density profiles for yeast membranes

estimated from the volume probability distributions of water and the average hydrocarbon tails region in each membrane. Figure 9 shows sample curves for volume probabilities of the mentioned regions in TGN2; the dashed line is a visual aid to locate half of the probability for each curve. All these values are reported in Table 3 and were interpolated from the data to get a more accurate value.

The D_{HH} for the ER and TGN membranes are very similar, between 37.4 and 38.6 Å. Moreover, the difference in unsaturation fraction between ER1 (0.86) and ER2 (0.69), or between TGN1 (0.74) and TGN2 (0.79), does not play a relevant role in the head-to-head distance and bilayer thickness (D_B) of these membranes. These result was also observed in the SA values for these models, and especially their K_A had no statistical difference (refer to Table 2) possibly due to the unsaturation degree of TGN (0.74 and 0.79 for models 1 and 2 of this membrane) falling in between that of the ER models (0.69 and 0.86).

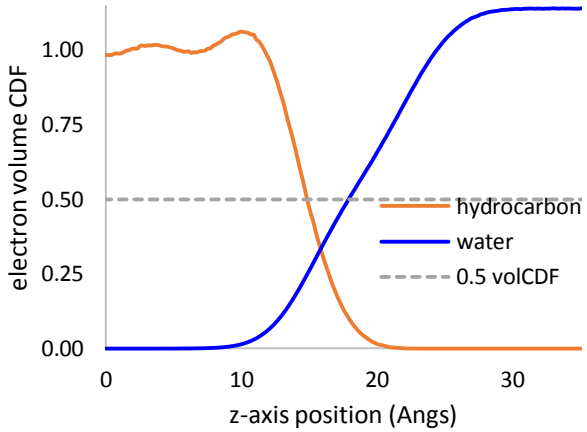

Figure 9 - Sample calculation of bilayer thickness (D_B) and hydrophobic core ($2D_C$) for TGN2

The content of PC lipids is also the highest if both membranes, and would occupy the same volume in both models. The ER and TGN are places of lipid exchange, and both contain the largest percentages of PC and PI lipids, while their ERG concentration is at least a quarter that of the PM membranes. The ordering effect of ERG is also noticeable in the PM and AVG-yeast EDPs, as these are bulkier membranes and their D_{HH} is 5-6 Å larger than the other two membranes. The same trend is observed in the D_B and $2D_C$ measurements.

Table 3 – Bilayer thicknesses of yeast membranes
Head-to-Head distance (D_{HH}), Bilayer thickness (D_B), and Hydrophobic core ($2D_C$)

Model	**D_{HH} (Å)**	**D_B (Å)**	**$2D_C$ (Å)**	**Exp.* (Å)**
er1	37.8 ± 0.1	34.42 ± 0.20	29.14 ± 0.20	30.8 ± 1.3 (*4cad*)
er2	37.4 ± 0.1	34.08 ± 0.20	29.30 ± 0.20	
tgn1	38.6 ± 0.1	36.44 ± 0.20	26.48 ± 0.20	n/a
tgn2	38.4 ± 0.1	35.82 ± 0.20	29.70 ± 0.20	
pm1	43.4 ± 0.1	39.34 ± 0.20	34.38 ± 0.20	29.8 ± 3.1 (*2k9p*)
pm2	44.4 ± 0.1	39.64 ± 0.20	34.88 ± 0.20	
avg-yeast	43.0 ± 0.1	39.88 ± 0.20	33.98 ± 0.20	n/a

(*http://opm.phar.umich.edu/protein.php?pdbid=4cad; http://opm.phar.umich.edu/protein.php?pdbid=2k9p)

The hydrophobic core thickness was used to compare the membranes with available experimental estimates taken from the Orientation for Proteins in Membranes (OPM) database that reports hydrophobic lengths of transmembrane proteins (56). Proteins for the ER and PM membranes are available in the database and reported in the last column of Table 3. The measurements are more reliable for the ER membrane because the hydrophobic length of the 4cad protein was estimated based on 8 helical subunits (57), while the PM transmembrane protein 2k9p had only 2 helical subunits (58). Despite limited experimental data, the ER estimates statistically agree with the experimental value of 30.8±1.3 Å, and the PM estimates are a slight overestimate but fall within 5% error with respect to experimental values.

3.3 Deuterium order parameters (S_{CD})

NMR experiments have been largely used to characterize the structure and order of lipids in pure and mixed bilayers, including mixtures with sterols (59). S_{CD}'s are segmental parameters that measure the order inside a bilayer, and are calculated for simulation data according to the angle between each C-D vector (bond) in the lipid tail and the bilayer normal, see Figure 10. Stereospecific nomenclature classifies the FA tails in lipids by their position with respect to the glycerol group. By convention, the FA in the *sn*-2 position is the one attached to the oxygen atom of the second carbon of the glycerol group; the other tail is named *sn*-1 chain. The hydrogens attached to the second carbon in the FA tails in the *sn-2* position give two different experimental signals that are also computed from the simulation data (60-64).

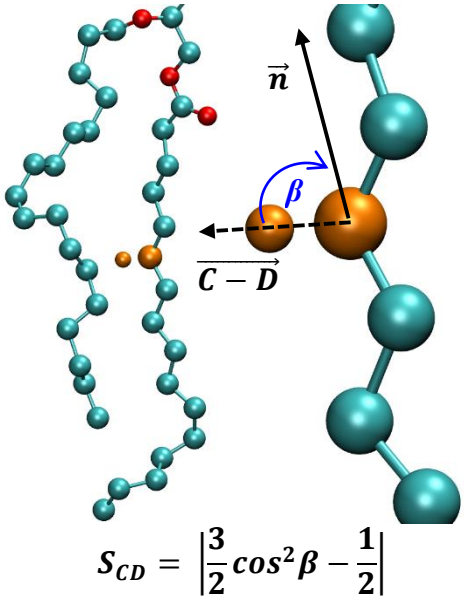

Figure 10 - S_{CD} parameters.
β is the angle between the C-D bond and the bilayer normal

Figures 11 to 13 show the S_{CD} values for each FA in the membrane lipids. It is clear at first glance that the S_{CD} values for the PM membranes, which contain the highest ERG concentration (40%), are higher than those of the ER or TGN models. This happens due to the presence of ERG in the leaflets that affects the lateral organization of lipids resulting in a more symmetric and bulkier bilayer (65). The AVG-yeast model also has high S_{CD} values and behaves more similarly to the PM than the other two models. Notice that the AVG-yeast model has a high CHL concentration of 22.2%, this sterol is more saturated

than ERG and could be the cause of having a more ordered bilayer than the ERs and TGNs even at this moderate concentration. The relative composition of DOPC-DPPC-CHOL from AVG-yeast in a ternary phase diagram lies in the L_d region at 303.15 K (66), but the dynamics introduced by the other lipids in the model, which have one saturated tail, may drive the overall mixture closer to the L_o stable region resulting in a more ordered bilayer with similar behavior to the PM models. In addition, the FA in the AVG-yeast and PM models have an average unsaturation fraction of 0.72 and 0.67 respectively, while the ER and TGN models' fractions range between 0.69 and 0.86. With higher concentration of unsaturated FAs, the bilayer core is more disordered because of the kinks double bonds introduce in the lipid tails conformation.

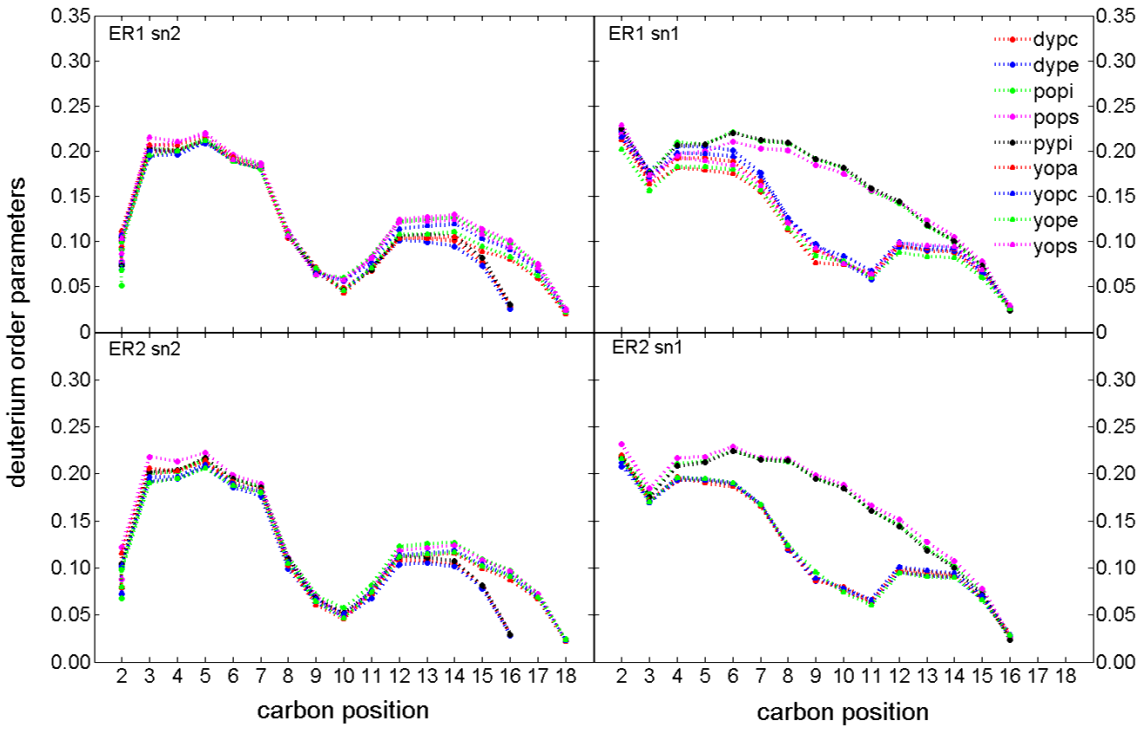

Figure 11 – S_{CD} parameters for the ER models 1 (top) and 2 (bottom)

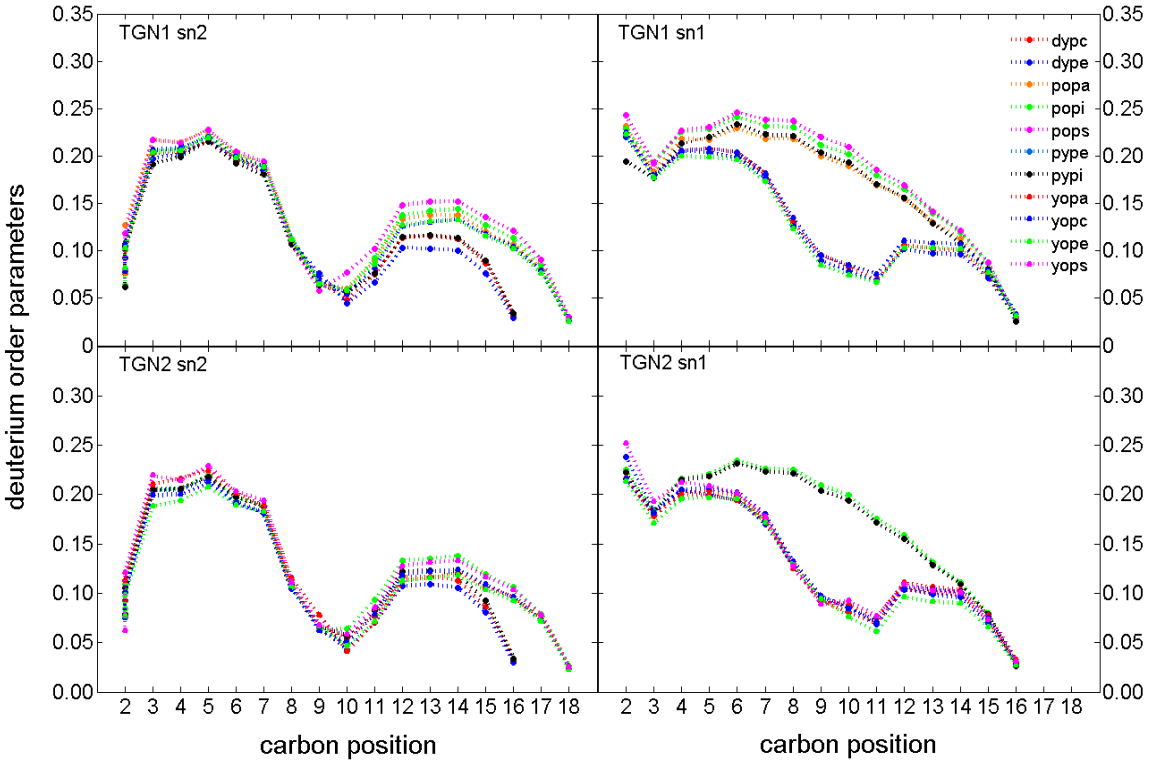

Figure 12 - S_{CD} parameters for the TGN models 1 (top) and 2 (bottom)

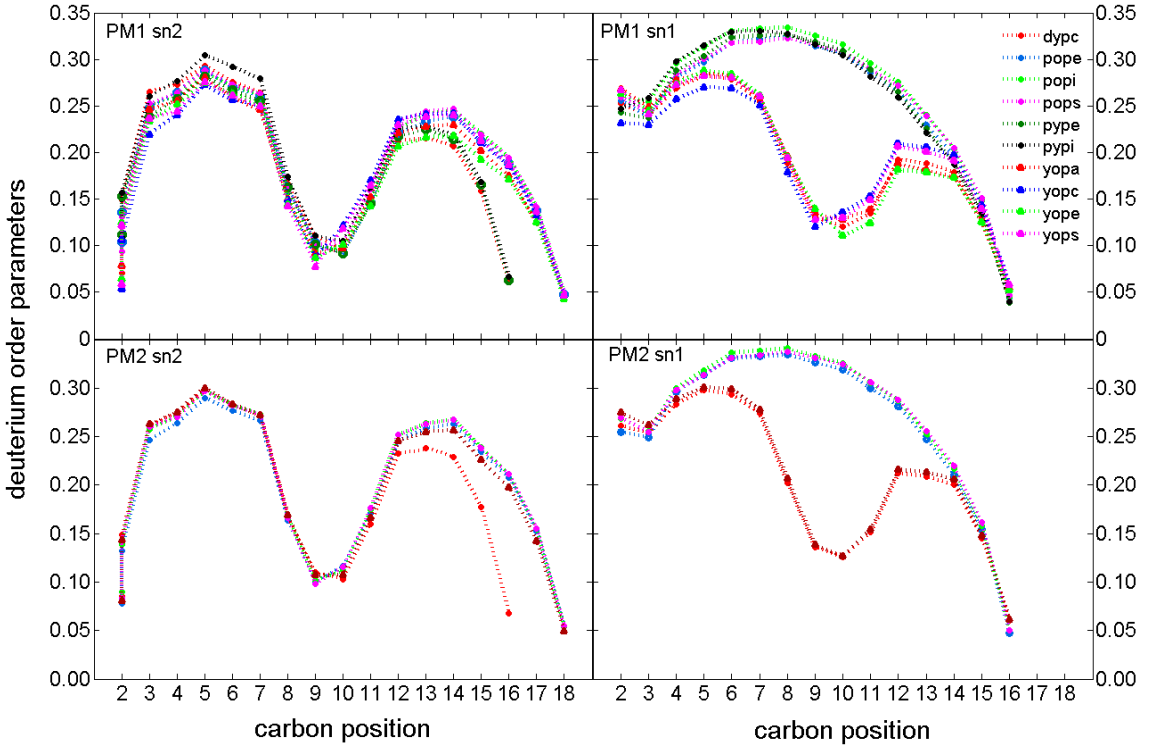

Figure 13 - S_{CD} parameter for the PM models 1 (top) and 2 (bottom)

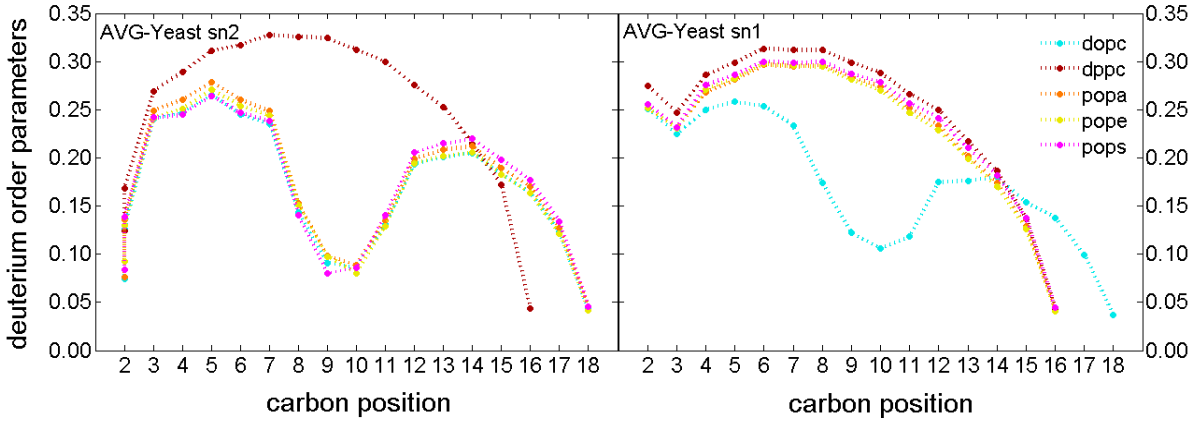

Figure 14 - S_{CD} parameters for the AVG-Yeast model

3.4 Lipid wobble rotation – NMR relaxation times (T_1)

NMR relaxation parameters give an insight on a bilayer's lipid motions and fluctuations (59). Rotational diffusion time constants are of special interest in computational models to determine the environment inside a bilayer. These relaxation times are measured by the second rank reorientational correlation function *C2(t)* for specific atoms in the simulation data, and could be validated against experimental data from NMR experiments if available (67). The correlation function is computed using vectors between selected atoms in the molecule of interest to determine its rotational diffusion rates. The vectors in this study were selected to estimate the slow relaxation time (wobble) between the first carbons of each FA tail (C22-

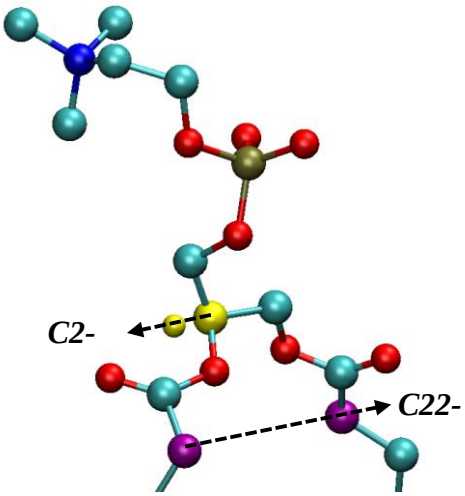

Figure 15 – Lipid wobble

Vectors used to compute glycerol carbon (yellow) and the cross-chain (purple) correlation functions for all the lipids in the yeast membranes. Colored atoms represent carbon (cyan), nitrogen (blue), oxygen (red), and phosphorus (gold).

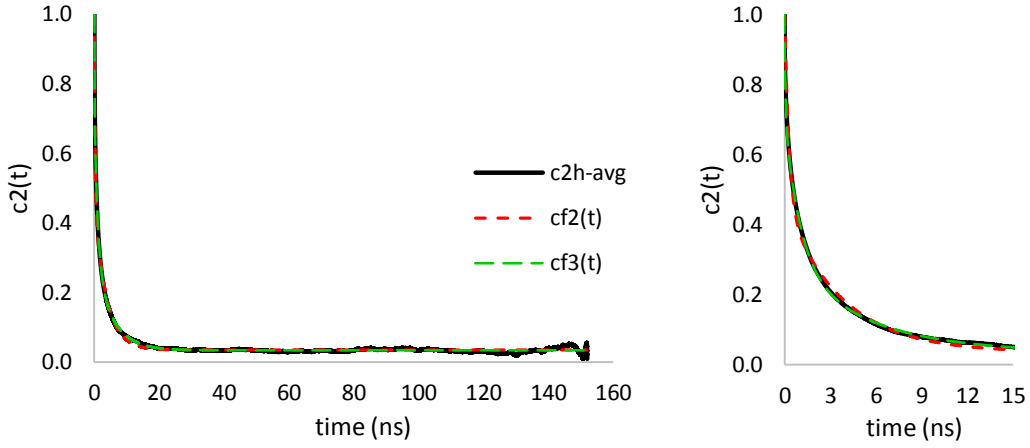

Figure 16 - Correlation function c2(t) for the second glycerol carbon in DYPC lipids of an equilibrated ER2 system (left) and close-up of the exponential decay section (right)

C32), and the second carbon of the glycerol group with its corresponding hydrogen (C2-HS), refer to Figure 15. Two and three exponential fits were obtained to determine time constants for each lipid type in the membranes; equation 7 shows the general form of the fitting function.

$$C2(t) = a_o + \sum_{i=1}^{3} a_i e^{-t/\tau_i} \qquad \textbf{(7)}$$

The independent coefficient a_o in equation 7, was estimated from the average value of the plateau reached by the correlation function over at least 100 ns (see Figure 16). The time constants in this equation represent the fast and slow relaxation times associated with the lipid's fast double bond isomerization and wobble respectively (63).

Tables 4 contains the average time constants for each model from two and three exponential fittings (Equation 7) for the second carbon of glycerol (CG); and Table 5 the average time constants for the cross-chain (CC) correlation function. The slow relaxation times, τ_2 for the two exponential fitting and τ_3 for the three exponential fitting, are characteristic times of lipid wobble in each model.

As expected, the PM membranes have longer wobble times compared to the other, while the ER membranes have the fastest times. This occurs due to the ordering effect of ERG molecules on each membrane. The range of CC relaxation times (6-17 ns), which provide a better idea of lipid wobble, is larger than the range for CG times (3-14 ns), indicating that the headgroups are more free to move than the lipid tails in a bilayer.

Table 4 – Relaxation times for the second carbon of glycerol correlation.
Average time constants for 2 and 3 exponential fittings; the standard error is in parentheses.

	CG-c2(t) - 2exp			**CG-c2(t)-3exp**		
model	**τ1 (ns)**	**τ2 (ns)**		**τ1 (ns)**	**τ2 (ns)**	**τ3 (ns)**
er1	0.28 *(0.03)*	3.90 *(0.33)*		0.05 *(0.02)*	0.90 *(0.18)*	5.10 *(0.72)*
er2	0.29 *(0.03)*	3.90 *(0.28)*		0.07 *(0.02)*	1.09 *(0.22)*	5.53 *(0.93)*
pm1	0.39 *(0.04)*	6.91 *(0.64)*		0.12 *(0.03)*	2.00 *(0.40)*	13.59 *(2.27)*
pm2	0.44 *(0.03)*	7.89 *(0.46)*		0.09 *(0.01)*	1.54 *(0.25)*	10.07 *(1.42)*
tgn1	0.33 *(0.05)*	4.66 *(0.72)*		0.07 *(0.02)*	1.13 *(0.32)*	6.92 *(0.76)*
tgn2	0.34 *(0.04)*	4.74 *(0.48)*		0.10 *(0.02)*	1.62 *(0.36)*	8.99 *(1.96)*
avg-yeast	0.33 *(0.03)*	4.78 *(0.36)*		0.10 *(0.02)*	1.24 *(0.31)*	6.63 *(1.16)*

The values reported in the table above are average values between the relaxation times of each lipid in a given model. The environment in a membrane is determined by its lipid components, unsaturation degree, and sterol fraction. Although there is no statistical difference in the wobble times between the two models for each organelle, the lipids with greater contribution in the longer, or shorter, average relaxation time did vary. For example, in PM1 the PIs were lipids with longer relaxation times in the case of CG, but the YO-lipids, with palmitoleic (C16:1) and oleic (C18:1) FAs, had the longest relaxation times for the CC correlation functions. On the other hand, the PM2 lipids had all similar relaxation times for both correlation functions. It is interesting to note that the AVG-Yeast membrane

had values more similar to the TGN membranes than to the PM, as was the case with the order parameters and EDPs. This occurs because the sterol content in AVG-yeast is closer to that of the TGN membranes, and it is also a simpler membrane in terms of lipid diversity than the PM.

Table 5 – Relaxation times for the cross-chain correlation.
Average time constants for 2 and 3exponential fittings; the standard error is in parentheses

	cross-c2(t)-2exp			**cross-c2(t)-3exp**		
model	**τ1 (ns)**	**τ2 (ns)**		**τ1 (ns)**	**τ2 (ns)**	**τ3 (ns)**
er1	0.45 *(0.05)*	6.58 *(0.72)*		0.13 *(0.01)*	1.53 *(0.15)*	8.51 *(0.70)*
er2	0.51 *(0.05)*	7.07 *(0.64)*		0.15 *(0.02)*	1.88 *(0.27)*	9.70 *(1.90)*
pm1	0.69 *(0.11)*	15.68 *(2.67)*		0.16 *(0.07)*	2.21 *(0.60)*	16.85 *(3.11)*
pm2	0.57 *(0.08)*	14.93 *(2.11)*		0.16 *(0.03)*	2.16 *(0.55)*	16.27 *(2.55)*
tgn1	0.56 *(0.07)*	8.28 *(1.39)*		0.17 *(0.03)*	2.16 *(0.38)*	12.05 *(1.56)*
tgn2	0.57 *(0.10)*	8.70 *(0.93)*		0.17 *(0.10)*	2.14 *(0.62)*	11.50 *(1.50)*
avg-yeast	0.53 *(0.08)*	9.46 *(1.47)*		0.16 *(0.03)*	1.81 *(0.35)*	11.72 *(1.47)*

CHAPTER 4 – BROADER DISCUSSION AND CONCLUSION

Six membrane models were built for three organelles in yeast *Saccharomyces cerevisiae* to study the effects of lipid saturation and diversity on the mechanical properties of the bilayer. Two membranes with different lipid unsaturation degrees, but identical head group distribution, were built to emulate the environment of the ER, TGN, and PM bilayers. Each membrane composition was tailored to mimic available experimental data that characterizes the lipid content of each organelle. All the bilayers were built using CHARMM-GUI *Membrane Builder* (39, 40), a user friendly interface that has recently updated its lipid library to over 200 molecules to include inositol lipid parameters among others. Three trajectories of 200 ns each were run using the CHARMM C36 FF (28, 29) on NAMD software package for each membrane to perform a more robust data analysis.

An initial study from Klauda and co-workers looked at the effect of sterol and lipid unsaturation on the surface area per lipid, electron density profiles, deuterium order parameters, an sterol tilt angle (15). The current thesis focused on the same properties, except the sterol tilt angle, plus the compressibility modulus (K_A) and rotational diffusion time constants for each model. The values were evaluated against each other, and only the bilayer thickness as estimated from the EDP was compared against experimental data available at the OPM database (56). One last membrane model was constructed based on the composition of Jo *et al.* (15) to compare its bilayer properties to those for organelle-specific models. As the results in this study confirm, the lipid composition of a membrane alters its environment and determines the extent of interactions with other membranes and proteins.

The surface area of a bilayer is a basic property mainly used to determine when the system has reach thermodynamic equilibrium or whether a phase transition occurs in the bilayer. The SA also provides information about the lipid packing in a bilayer; high SA values as those of the ER membranes, 63.99±0.38 and 63.65±0.36 $Å^2$, suggest the lipids occupy more space compared to those in the PM or AVG-yeast membranes, which SAs are around 47 $Å^2$. The SA was used to calculate the K_A, or membrane stiffness, for each bilayer that measures how easily the membrane can be compressed. It is interesting to note that despite their similar SA value, the AVG-yeast membrane is less stiff than the PM as shown by this membrane's K_A of 0.34 N/m. Higher values of K_A like those for the PM membranes (0.57 and 0.47 N/m) indicate a more rigid bilayer versus the smaller values for the more fluid ER and TGN membranes (~0.28 N/m). The difference was expected given the PM is the outermost membrane with high lipid packing density, while the ER and TGN are more flexible, loosely packed, lipid bilayers with more complex shapes than the PM (2).

The bilayer thickness calculated in this work were determined following the procedure described by Kučerka *et al.* (53, 55). Three characteristic thicknesses were determined for each model, D_H, D_B, and $2D_C$. D_H was estimated from the distance between peaks of the total EDP, including water, of each membrane – shown in Figure 8. The ER and TGN membranes follow basically the same EDP with minimal differences at the center of the bilayer. On the other hand, the PM membranes show lower electron density towards the center of the bilayer, related to the high sterol content and its ordering effect that prevents interdigitation of methyl groups from the bilayer top and bottom leaflets. The AVG-yeast membrane follows a similar trend, but has an overall lower density profile. The lower value may arise from the sterol ordering effect that also prevents interdigitation of tails in the

leaflets, but also from the average chain length in this membrane (28.75) that is the lowest among all the membranes in this work.

The estimates for D_B and $2D_C$ were calculated from half of the volume probability of the water and hydrocarbon EDPs respectively (refer to Figure 9). There is no statistical difference for these values between the PM and AVG-yeast membranes, but the ER has lower values than the TGN and both of these are thinner than the PM. In addition, the PM EDPs reflect tighter lipid packing versus the more relaxed case of the disordered ER and TGN bilayers. The values estimated from the simulation data were compared to hydrophobic core thickness for the ER and PM membranes available at the OPM database from transmembrane proteins data, and found within 5% error of the experimental values.

The S_{CD} parameters were used to study the order and structure of each bilayer. This parameter is expected to decrease going down the acyl chain (33), and have lower values in the presence of double bonds. Furthermore, the S_{CD} values are expected to be higher for ordered bilayers, like those with high sterol content. The membranes studied in this work correspond to the expected trend in the order parameters. The S_{CD}'s are at least 20% lower for the ER and TGN membranes with respect to the PM because of the loose packing of lipids and low sterol content, while the PM and AVG-yeast membranes have higher parameters for corresponding lipids between models.

Lastly, the rotational motions of each bilayer were studied calculating the slow relaxation times of rotation, or wobble, for each lipid with respect to the bilayer normal. The slow component of rotational motion is a limiting timescale for lipid motions inside the bilayer. This timescale gives an idea of lipid packing and interaction with its surroundings. The

values obtained for the membranes in this study are of the expected order of magnitude, and increase with the increase of sterol content in the bilayer. The ER membranes have the lowest values for lipid wobble, with an average of 9.1 ns as computed from the CC correlation function. On the other extreme, the lipid wobble in the PMs is on average 16.6 ns. Although in previous properties the AVG-Yeast membrane followed the same trend as the PM, its lipid wobble is closer to the range of the TGN membranes because they both have similar moderate ERG content. No significant statistical difference was observed between the relaxation times of the two models for each organelle.

In terms of agreement with other studies, the values reported in Tables 4 and 5 are of the expected order of magnitude. A previous study reported CG relaxation times for pure DPPC and PSM (a sphingolipid) bilayers (68); the tail length in sphingolipids may induce interdigitation in the bilayer and its structure is usually stabilized by inter-lipid hydrogen bonds, resulting in a more restricted environment for lipid rotation and longer relaxation times than the simple FA tails studied in this work. Our relaxation times are in between those reported in the article by Venable *et al.*; they are 3 times larger than those of pure DPPC bilayers because the present membranes have a sterol component, but are approximately five times smaller than the values of the sphingolipid system since our systems do not have inter-lipid hydrogen bonding.

The analysis in this thesis lead us to better understand the effect and importance of lipid composition on membrane properties. We hope to use these models to expand our understanding on membrane-protein interactions, and continue to improve our representation of organelle diversity as new FF parameters become available (68); the future directions of this project are detailed in the next chapter.

CHAPTER 5 – FUTURE DIRECTIONS

Organelle-specific models are needed to study specific membrane functions and interactions with both transmembrane and peripheral proteins through simulations. The goal of this work was to develop accurate representations for the ER, TGN, and PM in yeast and use these models in future studies of lipid nano-domains and lipid-protein interactions - both applications are described below in separate sections for clarity.

5.1 Long PM runs (Anton Machine)

Lipid rafts have gained attention in the past twenty years and have been identified as key players in membrane signaling processes. Sterol-rich domains have been mostly found with bilayers containing fully saturated lipids, like DPPC, and sphingolipids. The formation of these domains has recently also been associated with membrane curvature, and may form as a signaling platform when needed by the cell (24, 69).

The PM1 membrane run was extended to 5μs to study the formation and role of ERG clusters over time. Three replicate runs were carried on the Anton machine at Pittsburgh Supercomputing Center using the same cut-offs for the simulation parameters as the CHARMM runs. Transient ERG clusters were observed after 250ns, and an ERG flip was observed in each trajectory within the first microsecond of simulation. The flip was observed in cases where the opposite leaflet had a slightly higher degree of saturation such as more ERG lipids or lipids with palmitic (C16:0) and stearic (C18:0) FAs. Our goal is to characterize these nano-domains and determine their formation timescale. Additional membrane-only systems will be run using the most recent C36 FF that includes sphingomyelin and ceramide lipid parameters, both of which are mostly located at the PM

and play important roles in lipid raft formation (6, 68). Different membrane dynamics are expected for models with sphingolipids because they contain fully saturated tails that would interact with sterols forming lipid-rafts. The dynamics and timescale of this phenomenon are of special interest for the study of membrane-protein interactions.

5.2 Osh4 studies

The fact that most lipids are synthesized at the ER but are ultimately located at the other end of the secretory pathway suggests they are transported across organelles. Such transport has been suggested to occur in both vesicular and non-vesicular manners by means of membrane contact sites or LTPs (6). The peripheral protein Osh4, a member of a family of seven homologue oxysterol binding proteins in yeast, is an LTP. It was previously shown, using molecular dynamics simulations, that Osh4 has six membrane binding regions (18). Non-specific interactions with anionic lipids are an important driving force for the Osh4 attraction to yeast membranes. The ALPS-like motif of Osh4, a 29 amino acid peptide which also forms the lid to protect sterols, has also been identified as a membrane curvature sensor (70). We will characterize the binding mechanism of the peptide with bilayers containing different lipid types is described in terms of hydrogen bonding, peptide-bilayer distance, protein structure changes, and binding energies. Preliminary runs with CHARMM (200ns) and the Anton machine (2μs) have successfully seen the peptide steadily bind to simple membranes in two conformations with SER8 and LYS15 as recurrent binding residues. We plan to extend this study to use one of the ER and TGN membranes to study in more detail the binding mechanism of the full protein presenting its mouth open conformation to the membrane in the hope to learn the precise mechanism of sterol, or PI lipid, uptake for transport.

List of Publications

Published

1. Wu, E.L.; Cheng, X.; Jo, S.; Rui, H.; Song, K.C.; Davila-Contreras, E.M.; Qi, Y.; Lee, J.; Monje-Galvan, V.; Venable, R.M.; Klauda, J.B.; Im, W. 2014. CHARMM_GUI *Membrane Builder* toward Realistic Biological Membrane Simulations. *J. Comput. Chem*. 35(27), 1997-2004. DOI: 10.1002/jcc.23702
2. Jeong, J.C.; Jo, S.; Wu, E.L.; Qi, Y.; Monje-Galvan, V.; Yeom, M.S.; Gorenstein, L.; Chen, F.; Klauda, J.B.; Im, W. 2014. ST-Analyzer: A web-based user interface for simulation trajectory analysis. *J. Comput. Chem.* 35(12), 957-963. DOI: 10.1002/jcc.23584
3. Klauda, J.B.; Monje, V.; Kim, T.; Im, W. 2012. Improving the CHARM Force Field for Polyunsaturated Fatty Acid Chains. *J. Phys. Chem. B*. 116(31), 9424-9431.

To be submitted

4. Molecular dynamic simulations on organelle-specific yeast membrane models. December 2014. Viviana Monje-Galvan, Jeffery B. Klauda.
5. Effects of cholesterol composition on pure DOPC and DMPC bilayers. January 2015. Christopher Boughter, Jeffery B. Klauda, Viviana Monje-Galvan.
6. Membrane binding of the Osh4 curvature-sensing ALPS-like motif, a comprehensive MD study. March 2015. Viviana Monje-Galvan, Jeffery B. Klauda.

List of Conference Presentations

Delivered

1. XL Congress of Theoretical Chemists of the Latin Expression QUITEL 2014 (talk in Spanish). Galapagos, Ecuador; November 2014. Membrane binding of a curvature-sensing peptide of a lipid transport protein in yeast. Viviana Monje-Galvan, Jeffery B. Klauda. ISBN: 978-9978-68-070-4 (p.19)
2. 58th Biophysical Society National Meeting (poster session). San Francisco, CA 2014. Molecular dynamic studies on organelle-specific yeast membrane models and amphipathic lipid packing sensor motif binding mechanism. Viviana Monje-Galvan, Jeffery B. Klauda. DOI: 10.1016/j.bpj.2013.11.3916
3. 58th Biophysical Society National Meeting (poster session). San Francisco, CA 2014. St-Analyzer: A web-based user interface for simulation trajectory analysis. Jong Cheol Jeong, Sunhwan Jo, Emilia L Wu, Yifei Qi, Viviana Monje, Min Sum Yeom, Lev Goresntein, Feng, Chen, Jeffery B. Klauda, Wompil Im. DOI: 10.1016/j.bpj.2013.11.2291
4. AIChE National Meeting (talk #261c). San Francisco, CA 2013. Simulation studies on organelle-specific yeast membrane models and amphipathic lipid packing sensor motif binding mechanism. Viviana Monje-Galvan, Jeffery B. Klauda.
5. Oral contribution at the Universidad Mayor de San Andres, Instituto de Investigaciones Físicas (*Institute of Physics Research* – talk in Spanish). La Paz, Bolivia; March 2013. Mejorando el campo de fuerza para simulaciones moleculares de ácidos grasos poli-insaturados en membranas celulares. Viviana Monje, Jeffery B. Klauda.
6. 57th Biophysical Society National Meeting (poster session). Philadelphia, PA 2013. Improved CHARMM Force Field for Polyunsaturated Fatty Acid Chains, a Study on DAPC Membranes. Viviana Monje, Taehoon Kim, Wompil Im, Jeffery B. Klauda. DOI: 10.1016/j.bpj.2012.11.3277

Scheduled

7. 59th Biophysical Society National Meeting (poster session). February 7-11, 2015; Baltimore, MD. Membrane binding of the Osh4 curvature-sensing peptide. Viviana Monje-Galvan, Jeffery B. Klauda.

Under review

8. 249th American Chemical Society National Meeting (talk). March 22-26, 2015; Denver, CO. Binding studies of a *Saccharomyces cerevisiae* peripheral protein Osh4. Viviana Monje-Galvan, Jeffery B. Klauda

CHAPTER 6 - REFERENCES

1. Humphrey, W., A. Dalke, and K. Schulten. 1996. VMD: Visual molecular dynamics. Journal of Molecular Graphics 14:33–38.
2. van Meer, G., D. R. Voelker, and G. W. Feigenson. 2008. Membrane lipids: where they are and how they behave. Nature Reviews Molecular Cell Biology 9:112-124.
3. Fletcher, D. A., and R. D. Mullins. 2010. Cell mechanics and the cytoskeleton. Nature 463:485-492.
4. Engelman, D. M. 2005. Membranes are more mosaic than fluid. Nature 438:578-580.
5. Nelson, D. L., and M. M. Cox. Principles of Biochemistry. W.H. Freeman and Company, New York.
6. Klug, L., and G. Daum. 2014. Yeast lipid metabolism at a glance. FEMS Yeast Research 14:369-388.
7. Maxfield, F. R. T., Ira. 2005. Role of cholesterol and lipid organization in disease. Nature 438:612-621.
8. Rest, M. E. v. d., A. H. Kamminga, A. Nakano, Y. Anraku, B. Poolman, and W. N. Konings. 1995. The plasma membrane of Saccharomyces cerevisiae: structure, function, and biogenesis. Microbiology and Molecular Biology Reviews 59:304-322.
9. Klemm, R. W., C. S. Ejsing, M. A. Surma, H.-J. Kaiser, M. J. Gerl, J. L. Sampaio, Q. d. Robillard, C. Ferguson, T. J. Proszynski, A. Shevchenko, and K. Simons. 2009. Segregation of sphingolipids and sterols during formation of secretory vesicles at the trans-Golgi network. The Journal of Cell Biology 185:601-612.
10. Santos, A. X. S., and H. Riezman. 2012. Yeast as a model system for studying lipid homeostasis and function. FEBS Letters.
11. Stryer, L. 1989. Molecular Design of Life. W.H. Freeman and Company, New York, USA.
12. Khalili-Araghi, F., J. Gumbart, P. Wen, M. Sotomayor, E. Tajkhorshid, and K. Schulten. 2009. Molecular dynamics simulations of membrane channels and transporters. Current Opinion in Structural Biology 19:128–137.
13. D'Angelo, G., M. Vicinanza, and M. A. De Matteis. 2008. Lipid-transfer proteins in biosynthetic pathways. Current Opinion in Cell Biology 20:360–370.
14. Simons, K., and E. Ikonen. 2000. How Cells Handle Cholesterol. Science 290:1721-1726.
15. Jo, S., J. B. Lim, J. B. Klauda, and W. Im. 2009. CHARMM-GUI Membrane Builder for mixed bilayers and its application to yeast membranes. Biophys J 97:50-58.
16. Vanegas, J. M., M. F. Contreras, R. Faller, and M. L. Longo. 2012. Role of unsaturated lipid and ergosterol in ethanol tolerance of model yeast biomembranes. Biophys J 102:507-516.
17. Collins, M. D. 2008. Interleaflet Coupling Mechanisms in Bilayers of Lipids and Cholesterol☆. Biophys J 94:L32-34.

18. Rogaski, B., and J. B. Klauda. 2012. Membrane-Binding Mechanism of a Peripheral Membrane Protein through Microsecond Molecular Dynamics Simulations. Journal of Molecular Biology 423:847-861.
19. Fagone, P., and S. Jackowski. 2009. Membrane phospholipid synthesis and endoplasmic reticulum function. Journal of Lipid Research 50:S311-S316.
20. Chen, S., P. Novick, and S. Ferro-Novick. 2013. ER structure and function. Current Opinion in Cell Biology 25:428–433.
21. English, A. R., N. Zurek, and G. K. Voeltz. 2009. Peripheral ER structure and function. Current Opinion in Cell Biology 21:596-602.
22. Bankaitis, V. A., R. Garcia-Mata, and C. J. Mousley. 2012. Golgi Membrane Dynamics and Lipid Metabolism. Current Biology 22:R414-424.
23. Leber, A., C. Hrastnick, and G. Daum. 1995. Phospholipid-synthesizing enzymes in Golgi membranes of the yeast, Saccharomyces cerevisiae. FEBS Letters 377:271-274.
24. Bastos, A. E. P., H. S. Marinho, A. M. Cordeiro, A. M. de Soure, and R. F. M. de Almeida. 2012. Biophysical properties of ergosterol-enriched lipid rafts in yeast and tools for their study: characterization of ergosterol/phosphatidylcholine membranes with three fluorescent membrane probes. Chemistry and Physics of Lipids 165:577-588.
25. Tuller, G., T. Nemec, C. Hrastnik, and G. Daum. 1999. Lipid composition of subcellular membranes of an FY1679-derived haploid yeast wild-type strain grown on different carbon sources. Yeast 15:1555-1564.
26. Leach, A. R. 2001. Molecular Modeling Principles and Applications. Pearson Education, Great Britain.
27. Frenkel, D., and B. Smit. 2001. Understanding Molecular Simulation From Algorithms to Applications. Academic Press.
28. Klauda, J. B., R. M. Venable, J. A. Freites, J. W. O'Connor, D. J. Tobias, C. Mondragon-Ramirez, I. Vorobyov, A. D. MacKerell, and R. W. Pastor. 2010. Update of the CHARMM all-atom additive force field for lipids: Validation on six lipid types. J Phys Chem B 114:7830-7843.
29. Lim, J. B., B. Rogaski, and J. B. Klauda. 2011. Update of the Cholesterol Force Field Parameters in CHARMM. The Journal of Physical Chemistry B 116:203-210.
30. Darden, T., D. York, and L. Pedersen. 1993. Particle mesh Ewald: An N·log(N) method for Ewald sums in large systems. The Journal of Chemical Physics 98.
31. Brooks, B. R., C. L. Brooks, A. D. Mackerell J., L. Nilsson, R. J. Petrella, B. Roux, Y. Won, G. Archontis, C. Bartels, S. Boresch, A. Caflish, L. Caves, Q. Cui, A. R. Dinner, M. Feig, S. Fischer, J. Gao, M. Hodoscek, W. Im, K. Kuczera, T. Lazaridis, J. Ma, V. Ovchinnikov, E. Paci, R. W. Pastor, C. B. Post, J. Z. Pu, M. Schaefer, B. Tidor, R. M. Venable, H. L. Woodcock, X. Wu, W. g. Yang, D. M. York, and M. Karplus. 2009. CHARMM: The biomolecular simulation program. Journal of Computational Chemistry 30:1545-1614.
32. Phillips, J. C., R. Braun, W. Wang, J. Gumbart, E. Tajkhorshid, E. Villa, C. Chipot, R. D. Skeel, L. Kale, and K. Schulten. 2005. Scalable molecular dynamics with NAMD. Journal of Computational Chemistry 26:1781-1802.

33. Pandit, K. R., and J. B. Klauda. 2012. Membrane models of E. coli containing cyclic moieties in the aliphatic lipid chain. Biochim Biophys Acta 1818:1205-1210.
34. Sandler, S. I. 2010. An Introduction to Applied Statistical Thermodynamics. John Wiley & Sons, Inc., USA.
35. Assael, M. J., A. R. H. Goodwin, M. Stamatoudis, W. A. Wakeham, and S. Will. 2011. Commonly Asked Questions in Thermodynamics. CRC Press, Taylor & Francis Group, USA.
36. Feller, S. E., Y. Zhang, R. W. Pastor, and B. R. Brooks. 1995. Constant pressure molecular dynamics simulation: The Langevin piston method. The Journal of Chemical Physics 103:4613-4621.
37. Martyna, G. J., D. J. Tobias, and M. L. Klein. 1994. Constant pressure molecular dynamics algorithms. The Journal of Chemical Physics 101:4177-4189.
38. Jo, S., T. Kim, V. G. Iyer, and W. Im. 2008. CHARMM-GUI: A web-based graphical user interface for CHARMM. Journal of Computational Chemistry 29:1859-1865.
39. Jo, S., T. Kim, and W. Im. 2007. Automated Builder and Database of Protein/Membrane Complexes for Molecular Dynamics Simulations. PLOS one:e880.
40. Wu, E. L., X. Cheng, S. Jo, H. Rui, K. C. Song, E. M. Davila-Contreras, Y. Qi, J. Lee, V. Monje-Galvan, R. M. Venable, J. B. Klauda, and W. Im. 2014. CHARMM-GUI Membrane Builder toward realistic biological membrane simulations. Journal of Computational Chemistry.
41. Daum, G., G. Tuller, T. Nemec, C. Hrastnik, G. Balliano, L. Cattel, P. Milla, F. Rocco, A. Conzelmann, C. Vionnet, D. E. Kelly, S. Kelly, E. Schweizer, J. Schüller, U. Hojad, E. Greiner, and K. Finger. 1999. Systematic analysis of yeast strains with possible defects in lipid metabolism. Yeast 15:601-614.
42. Schneiter, R., B. Brügger, R. Sandhoff, G. Zellnig, A. Leber, M. Lampl, K. Athenstaedt, C. Hrastnik, S. Eder, G. Daum, F. Paltauf, F. T. Wieland, and S. D. Kohlwein. 1999. Electrospray Ionization Tandem Mass Spectrometry (Esi-Ms/Ms) Analysis of the Lipid Molecular Species Composition of Yeast Subcellular Membranes Reveals Acyl Chain-Based Sorting/Remodeling of Distinct Molecular Species En Route to the Plasma Membrane. The Journal of Cell Biology 146:741-754.
43. Zinser, E., C. D. Sperka-Gottlieb, E. V. Fasch, S. D. Kohlwein, F. Paltauf, and G. Daum. 1991. Phospholipid synthesis and lipid composition of subcellular membranes in the unicellular eukaryote Saccharomyces cerevisiae. Journal of Bacteriology 173:2026-2034.
44. Jorgensen, W. L., J. Chandrasekhar, J. D. Madura, R. W. Impey, and M. L. Klein. 1983. Comparison of simple potential functions for simulating liquid water. The Journal of Chemical Physics 79.
45. Ryckaert, J.-P., G. Ciccotti, and H. J. C. Berendsen. 1977. Numerical integration of the cartesian equations of motion of a system with constraints: molecular dynamics of n-alkanes. Journal of Computational Physics 23:327–341.

46. Steinbach, P. J., and B. R. Brooks. 1994. New spherical-cutoff methods for long-range forces in macromolecular simulation. Journal of Computational Chemistry 15:667-683.
47. Essmann, U., L. Perera, M. L. Berkowitz, T. Darden, H. Lee, and L. G. Pedersen. 1995. A smooth particle mesh Ewald method. The Journal of Chemical Physics 103.
48. Hoover, W. G. 1985. Canonical dynamics: Equilibrium phase-space distributions. Physical Review A 31.
49. Nosé, S., and M. L. Klein. 1983. A study of solid and liquid carbon tetrafluoride using the constant pressure molecular dynamics technique. The Journal of Chemical Physics 78.
50. Arora, A., H. Raghuraman, and A. Chattopadhyay. 2004. Influence of cholesterol and ergosterol on membrane dynamics: a fluorescence approach ☆. Biochimica et Biophysica Acta (BBA) Reseach Communications 318:920–926.
51. Guo, Y., S. Pogodin, and V. A. Baulin. 2014. General model of phospholipid bilayers in fluid phase within the single chain mean field theory. J Chem Phys 140:174903.
52. Kučerka, N., M.-P. Nieh, and J. Katsaras. 2011. Fluid phase lipid areas and bilayer thicknesses of commonly used phosphatidylcholines as a function of temperature. Biochimica et Biophysica Acta (BBA) - Biomembranes 1808:2761–2771.
53. Kučerka, N., J. F. Nagle, J. N. Sachs, S. E. Feller, J. Pencer, A. Jackson, and J. Katsaras. 2008. Lipid bilayer structure determined by the simultaneous analysis of neutron and X-ray scattering data. Biophys J 95:2356-2367.
54. Pan, J., D. Marquardt, F. A. Heberle, N. Kučerka, and J. Katsaras. 2014. Revisiting the bilayer structures of fluid phase phosphatidylglycerol lipids: Accounting for exchangeable hydrogens. Biochim Biophys Acta 1838:2966-2969.
55. Kučerka, N., j. Katsaras, and J. F. Nagle. 2010. Comparing Membrane Simulations to Scattering Experiments: Introducing. Journal of Membrane Biology 235:43-50.
56. Lomize, M. A., A. L. Lomize, I. D. Pogozheva, and H. I. Mosberg. 2006. OPM: orientations of proteins in membranes database. Bioinformatics 22:623-625.
57. Neumoin, A., L. S. Cohen, B. Arshava, S. Tantry, J. M. Becker, O. Zerbe, and F. Naider. 2009. Structure of a double transmembrane fragment of a G-protein-coupled receptor in micelles. Biophys J 96:3187-3196.
58. Manolaridis, I., K. Kulkarni, R. B. Dodd, S. Ogasawara, Z. Zhang, G. Bineva, N. O'Reilly, S. J. Hanrahan, A. J. Thompson, N. Cronin, S. Iwata, and D. Barford. 2013. Mechanism of farnesylated CAAX protein processing by the intramembrane protease Rce1. Nature 504:301-305.
59. Leftin, A., and M. F. Brown. 2011. An NMR database for simulations of membrane dynamics. Biochim Biophys Acta 1808:818-839.
60. Seelig, A., and J. Seelig. 1974. Dynamic structure of fatty acyl chains in a phospholipid bilayer measured by deuterium magnetic resonance. Biochemistry 13:4839-4845.

61. Seelig, A., and J. Seelig. 1975. Bilayers of dipalmitoyl-3-sn-phosphatidylcholine. Conformational differences between the fatty acyl chains. Biochim Biophys Acta 406:1-5.
62. Seelig, J., and N. Waespe-Sarcevic. 1978. Molecular order in cis and trans unsaturated phospholipid bilayers. Biochemistry 17:3310-3315.
63. Klauda, J. B., N. V. Eldho, K. Gawrisch, B. R. Brooks, and R. W. Pastor. 2008. Collective and noncollective models of NMR relaxation in lipid vesicles and multilayers. J Phys Chem B 112:5924-5929.
64. Perly, B., I. C. Smith, and H. C. Jarrell. 1985. Acyl chain dynamics of phosphatidylethanolamines containing oleic acid and dihydrosterculic acid: 2H NMR relaxation studies. Biochemistry 24:4659-4665.
65. Simons, K., and E. Ikonen. 2000. How Cells Handle Cholesterol. Science 290:1721-1726.
66. Davis, J. H., J. J. Clair, and J. Juhasz. 2009. Phase equilibria in DOPC/DPPC-d62/cholesterol mixtures. Biophys J 96:521-539.
67. Klauda, J. B., M. F. Roberts, A. G. Redfield, B. R. Brooks, and R. W. Pastor. 2008. Rotation of Lipids in Membranes: Molecular Dynamics Simulation, 31P Spin-Lattice Relaxation, and Rigid-Body Dynamics. Biophysical Journal 94:3074-3083.
68. Venable, R. M., A. J. Sodt, B. Rogaski, H. Rui, E. Hatcher, A. D. MacKerell, R. W. Pastor, and J. B. Klauda. 2014. CHARMM All-Atom Additive Force Field for Sphingomyelin: Elucidation of Hydrogen Bonding and of Positive Curvature. Biophysical Journal Accepted.
69. Sadeghi, S., M. Muller, and R. L. C. Vink. 2014. Raft Formation in Lipid Bilayers Coupled to Curvature. Biophysical Journal 107:1591-1600.
70. Drin, G., J. F. Casella, R. Gautier, T. Boehmer, T. U. Schwartz, and B. Antonny. 2007. A general amphipathic alpha-helical motif for sensing membrane curvature. Nat Struct Mol Biol 14:138-146.